Materials Advances

ROYAL SOCIETY OF CHEMISTRY

REVIEW

View Article Online
View Journal | View Issue

Cite this: *Mater. Adv.*, 2021, 2, 4497

Recent advances on the removal of dyes from wastewater using various adsorbents: a critical review†

Soumi Dutta,[a] Bramha Gupta,[a] Suneel Kumar Srivastava *[b] and Ashok Kumar Gupta*[c]

The rapid increase in toxic dye wastewater generated from various industries remains a severe public health issue and prime environmental protection concern, posing a major challenge to existing conventional water treatment systems. Consequently, various physicochemical and biological treatment processes have been studied, which exhibit varying removal abilities depending on their experimental constraints. Among them, adsorption is considered to be the most efficient due to its high removal efficiency, easy operation, cost-effectiveness, and recyclability of the adsorbents. Considering this, the present review article focused on presenting a comprehensive summary of the various types of adsorbents such as commercial activated carbon, metal oxide-based, carbon-based, metal–organic framework, and polymer-based adsorbents used in dye remediation of contaminated water. The effects of several critical factors such as initial dye concentration, solution pH, temperature, and adsorbent dose on the dye adsorption performance are also described. In addition, the adsorption mechanisms responsible for dye removal are explained based on electrostatic attraction, ion exchange, surface complexation, and π–π interactions. Finally, critiques, future perspectives, and a summary of the present article are given. Various adsorbents such as carbon-based materials, metal oxides, bio-adsorbents, and polymer-based materials, have been shown to be efficient for the removal of dye pollutants from wastewater. Thus, it is anticipated that dye removal by adsorption can provide a feasible solution for the treatment of dye-laden water.

Received 17th April 2021,
Accepted 2nd June 2021

DOI: 10.1039/d1ma00354b

rsc.li/materials-advances

1. Introduction

The rapid growth of the global population, climate change, and industrial development has significantly affected water quality, resulting in an increasing freshwater crisis worldwide. Considering this, various consumers and polluters of freshwater significantly contribute to freshwater depletion.[1,2] Among them, the increasingly used dyes including methylene blue (MB), rhodamine B (RhB), methyl orange (MO), Congo red (CR), Disperse Violet 26, methyl red, and crystal violet are the most important sources of industrial pollutants originating from different industries such as the textile, cosmetic, leather, food, pharmaceutical, paint and varnish, and pulp and paper industries (Table 1).[3–16] According to a recent estimate, about 70 lakh tons of dyes are produced annually worldwide.[17] The release of this industrial waste dye into water jeopardizes human health and the environment. Consequently, research in this area is ongoing, which is obvious from the drastic upsurge in the number of research articles published on 'Dye Removal' in 2016–2020, as displayed schematically in Fig. 1.

The direct disposal of untreated dye-containing effluent into natural water bodies has an adverse effect on the photosynthetic activity in aquatic ecosystems.[18] It creates mutagenic or teratogenic effects on aquatic organisms and fish species due to the existence of metals[19] and aromatics.[20] Further, the presence of dyes in the environment has mild to severe toxic effects on human health, including carcinogenic, mutagenic, allergic, and dermatitis effects, kidney disease.[21] It has been reported that chromium-based dyes are generally complex in structure and cause carcinogenic effects on human health.[22] Thus, the disposal of dyes in the environment contaminates the water bodies, subsequently affecting the water quality, aquatic life, and human health. Table 1 also describes the ecotoxicological effects of dyes on living organisms. The sources and pathways of various dye pollutants in water bodies are depicted in Fig. 2.

[a] *School of Water Resources, Indian Institute of Technology Kharagpur, Kharagpur 721302, India*
[b] *Department of Chemistry, Indian Institute of Technology Kharagpur, Kharagpur 721302, India. E-mail: sunil111954@yahoo.co.uk*
[c] *Environmental Engineering Division, Department of Civil Engineering, Indian Institute of Technology Kharagpur, Kharagpur 721302, India. E-mail: agupta@civil.iitkgp.ac.in*

† Electronic supplementary information (ESI) available. See DOI: 10.1039/d1ma00354b

Table 1 Classification, examples, applications, solubility in water, and ecotoxicological effects of dyes

Type of dye	Example of chemical structure of dye	Examples of dyes	Dye application	Solubility in water	Ecotoxicological effects	Ref.
Acid dye	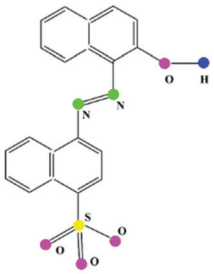 Acid red 88	Acid yellow 36, Acid orange 7, Acid blue 83, Acid blue 7	Textile, leather, and pharmaceutical industries; nylon, wool, silk, and modified acrylics	Water soluble	Vomiting, nausea, diarrhea, carcinogenic and mutagenic effects	3 and 72–75
Basic dye	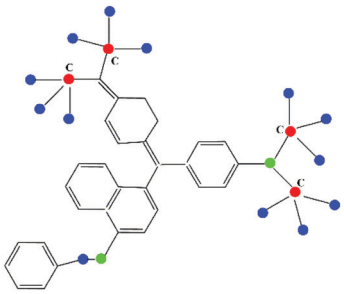 Basic blue 26	Methylene blue (MB), Basic red 1 or rhodamine 6G, Basic yellow 2	Paper, poly-acrylonitrile modified nylons, and modified polyesters	Water soluble	Altering the chemical and physical properties of water bodies and causing detrimental effects to the flora and fauna	3, 72, 76 and 77
Direct dye	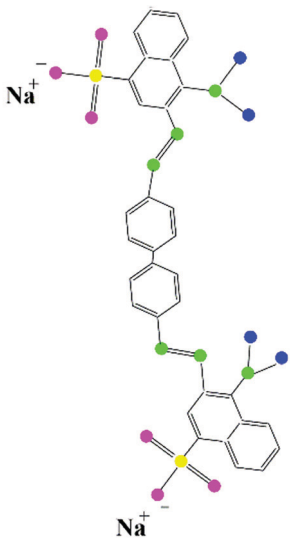 Direct red 28	Congo red (CR), Direct red 28, Direct black 38	Coloring paper products	Water soluble	Toxic to aquatic animals and plants; carcinogenic; mutagenic, and dermatitis	3, 72 and 78–80
Vat dye	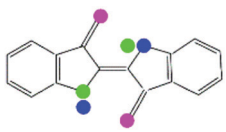 Vat blue 1	Vat blue 1, Vat acid blue 74	Insoluble pigment, indigo, and natural fibers, cellulosic fibers	Water insoluble	Severely affects the quality and clearness of water resources such as lakes and rivers; dermatitis, allergic conjunctivitis, rhinitis, and other allergic reactions	3, 72, 73, 76, 81 and 82
Disperse dye	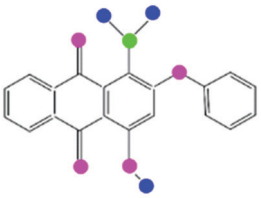 Disperse red 60	Disperse red 9, Disperse violet 1, Disperse red 60	Polyester, nylon, cellulose acetate, and acrylic fibers		Mutagenic; carcinogenic; causes soil and water pollution	3, 72 and 83

Table 1 (*continued*)

Type of dye	Example of chemical structure of dye	Examples of dyes	Dye application	Solubility in water	Ecotoxicological effects	Ref.
Nitro dye	 Chromophore of nitro dye	Naphthol yellow (II)	Dye wool		Decreases light penetration and photosynthetic activity; carcinogenic and mutagenic	3, 72 and 84
Mordant dye	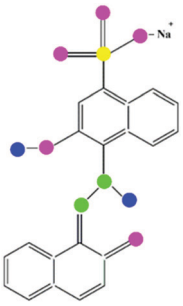 Mordant black 17	Mordant red 11, Mordant Black 17	Textile fibres such as wool, silk, and leather		Shows allergic reactions	3, 72, 85 and 86
Reactive dye	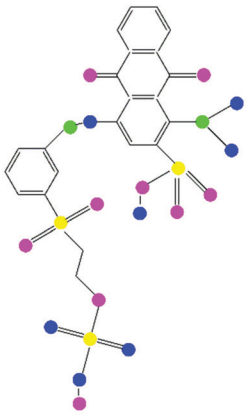 Reactive blue 19	C.I. reactive red 120, C.I. reactive red 147, C.I. reactive blue 19	Dyeing cellulosic, silk, and wool fibres		High and unwanted levels of dissolved solids in the effluent Allergic reaction in eyes, skin, mucous membrane, and the upper respiratory tract	3 and 72
Sulphur dye	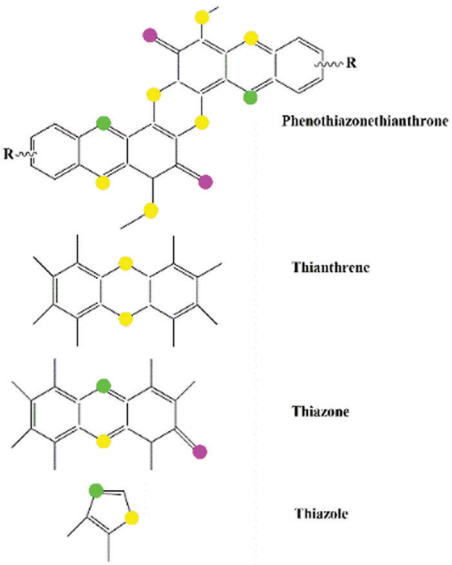 Phenothiazonethianthrone Thianthrene Thiazone Thiazole	Sulfur brilliant green, Sulfur blue, Sulfur Black 1, Leuco Sulfur Black 1, Phthalic anhydride	Dyeing cellulosic fibres and cotton	Water insoluble	Skin irritation; itchy or blocked noses; sneezing and sore eyes; carcinogenic	3, 72 and 76

Table 1 (*continued*)

Type of dye	Example of chemical structure of dye	Examples of dyes	Dye application	Solubility in water	Ecotoxicological effects	Ref.
Azo dyes	 **Chromophore of azo dyes**	Direct Black 22, Disperse Yellow 7, Acid Orange 20, Methyl red, Methyl orange (MO), Trypan blue	Textile industry for dyeing process and food coloring		Causes carcinogenicity in humans and animals. If inhaled or swallowed, it affects the eye, skin, and digestive tract. Affects aquatic life if present in excess.	3, 15, 72, 73 and 87–90

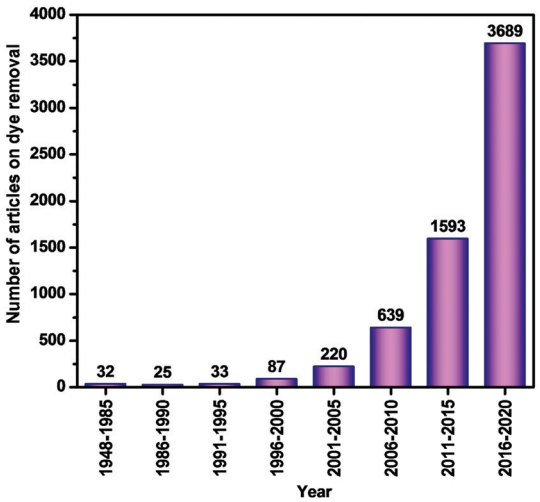

Fig. 1 Frequency of publications on dye removal with selected keyword 'Dye Removal' (details are given in Section A of the ESI†).

Accordingly, researchers have focused on the remediation of dye wastewater using coagulation/flocculation, electrocoagulation, filtration, adsorption, ion-exchange, advanced oxidation processes (AOPs), activated sludge processes (ASP), sequencing batch reactors (SBR), membrane bioreactors (MBR), moving bed biofilm reactors (MBBR), and constructed wetlands (CW).[23–30] The coagulation process involves the destabilization of charged suspended and colloidal impurities.[31,32] The electrocoagulation method employs a direct current source between metal electrodes containing iron or aluminum submerged in dye-contaminated water. Metal ions create a wide range of coagulated species and metal hydroxides at a certain pH, which destabilize and agglomerate suspended particles or precipitates and adsorb dye molecules.[23,33] In the filtration techniques, the separation of dissolved and suspended particles is carried out by sieving and particle capturing mechanisms.[32,34,35] Adsorption methods involve the movement of solids from the bulk liquid to the surface of the adsorbent.[26,36] The ion-exchange method involves the removal of dyes through the strong interactions between the functional groups on ion exchange resins and charged dye molecules.

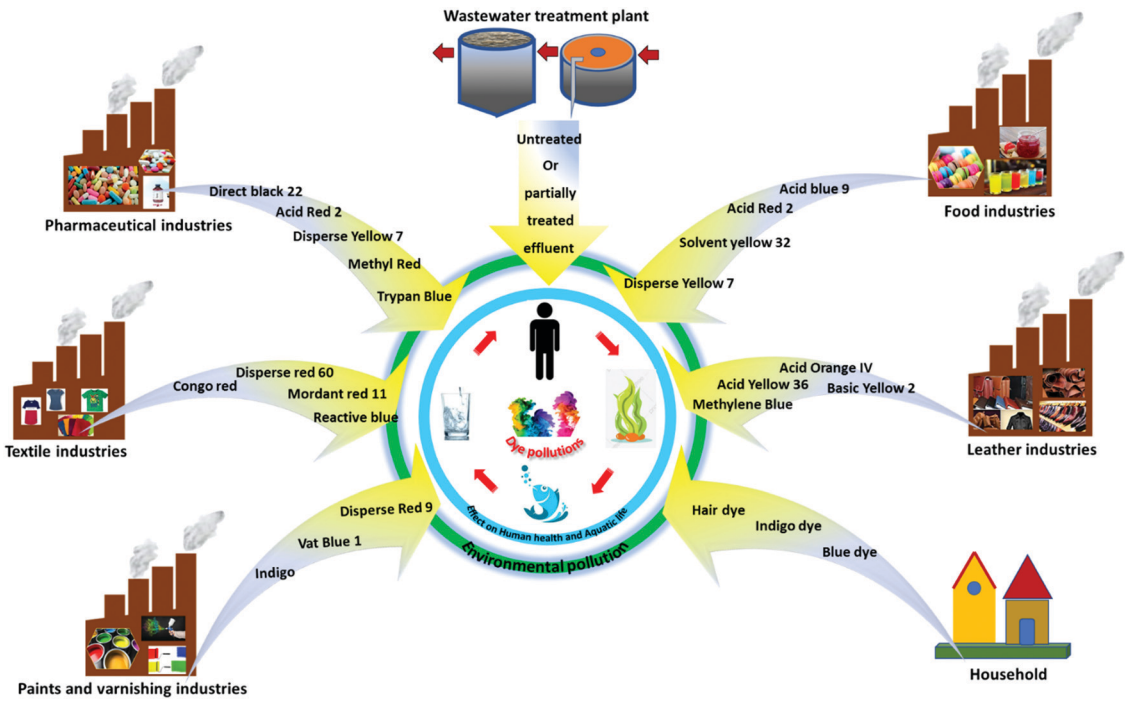

Fig. 2 Sources and pathways of dyes in the environment.

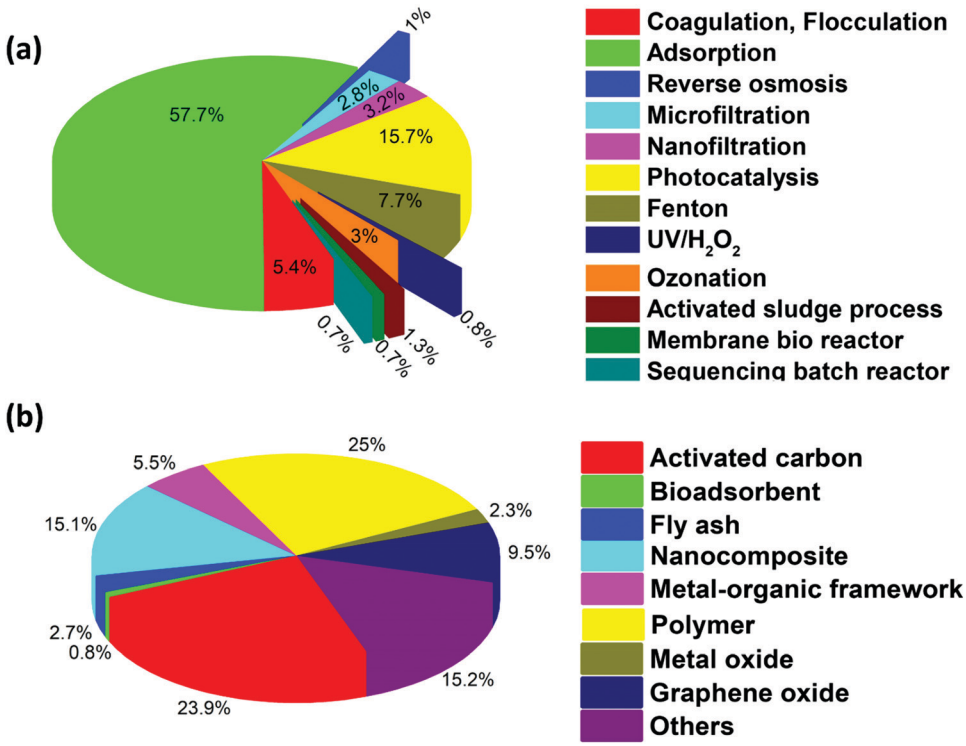

Fig. 3 Pie-chart showing the percentage of literature available on dye removal for (a) various physicochemical and biological techniques. Keywords: dye, water, treatment, and name of each technique, as mentioned in the plot. (b) Adsorption techniques using different adsorbents. Keywords: dye, water, adsorption, and the type of each adsorbent as mentioned in the plot. (Details are given in Section B and C of the ESI,† respectively).

The formation of strong linkages between the resins and the dye molecules results in the separation of dyes from wastewater.[29] The use of AOPs, such as ozonation, ultraviolet/hydrogen peroxide (UV/H_2O_2), Fenton, ultrasound, anodic oxidation, and photocatalytic processes, have been efficiently employed to treat dye wastewater. AOPs involve the formation of active radicals, which degrade targeted contaminants.[35,37–43] The suspended and/or attached growth of bacterial systems (*i.e.*, ASP, MBBR, SBR, CW, and MBR) have been employed in the biodegradation of dye molecules.[44,45] The number of articles on various existing physicochemical and biological treatment techniques is shown in Fig. 3a, which confirms that among these technologies, adsorption is considered to be one of the most important and useful decontamination processes. It is considered to be a fast, low cost, simple, sludge-free process, having high efficiency and/or selectivity, mechanical stability, and recycling facilities.[14,46–51] The adsorption process is widely used for the remediation of different pollutants from wastewater, including heavy metals, arsenic, and dyes.[52–59] Additionally, a pie chart displaying the percentage of literature available on dye removal using various adsorption techniques is shown in Fig. 3b. Considering this, the present study aims to review dye removal from polluted water *via* the adsorption process using various types of adsorbents. Specifically, several adsorbents, including activated carbon, metal oxide-based, carbon-based, bio-adsorbent, metal–organic framework (MOF), and polymer-based materials, are widely applied for the adsorption of dye from polluted water.[13,14,60–67] These adsorbents possess the advantages of easy fabrication, high effective surface area, multi-functionalities, high surface volume ratio, high reactivity, large number of active sites, reusability, low cost, and high efficiency to treat recalcitrant compounds.[68,69]

According to the available literature, several techniques such as chemical oxidation, coagulation, filtration with coagulation, precipitation, adsorption, and biological treatments have been frequently used to remove dyes from industrial and domestic effluents. However, the use of each of these methods in separation has merits and disadvantages. For example, coagulation is most commonly used method in industry, which does not involve the formation of harmful and toxic intermediates. However, inherent sludge formation and its disposal remain its biggest drawback. Further, the choice of method is also guided by operational costs. Considering this, the adsorption process is considered to be one of the most effective and inexpensive treatment processes to remove dyes in wastewater. Accordingly, the present article presents a review of the challenges and opportunities of the adsorption methodology available as the current state of the art in the removal of dyes from contaminated water. This covers the classification of dye effluents released from various industries, their solubility in water, chemical structures, and impact of these toxic compounds on the environment and human health, and the types of adsorbents used in the remediation of dyes are reviewed. This is followed by an updated review on the removal of different dyes using a variety of adsorbents. In addition, the adsorptive separation of dyes is also assessed in terms of the critical factors influencing dye separation, maximum adsorption capacity, adsorption mechanisms, and adsorption kinetics. It is anticipated that

the current review will be helpful in identifying cost-effective and efficient adsorption methods for the remediation of industrial dyes in wastewater. Finally, the present review also targets various research gaps and their possible solution.

2. Dyes: sources, classifications, and ecotoxicological effects

A dye is generally described as substances capable of imparting color through physical/chemical binding on a substrate to which it is applied. The presence of chromophores in dye accounts for the development of color, which auxochromes are attached to.[65] Table 1 describes the classification of dyes based on their physicochemical properties, applications, ecotoxicological effects, and water solubility. These dyes exhibit aromatic molecular structures originating from hydrocarbons, such as benzene, toluene, naphthalene, anthracene, and xylene.[70] Dyes are mainly derived from two significant sources, including natural and anthropogenic. The natural sources include plants, different insects, animals, and minerals, whereas synthetic dyes are man-made or manufactured using various organic molecules.[3,71] However, the multifaceted applications of dyes in daily life involve their release together with other toxic organic/inorganic chemicals from industrial effluents, resulting in detrimental effects on the environment.[71] Therefore, it is necessary to protect the environment from these toxic dye/dye effluents released in water by subjecting them to various physical, chemical, biological treatments or their combinations. Fig. 2 shows the sources and pathways of different dyes originating from various sources, such as industry, wastewater treatment plants and households, contributing to environmental pollution. Dyes can be classified considering their chemical structure, physicochemical attributes, origin, and applications.[22] This classification also considers the extremely hazardous/toxic industrial effluents that are carcinogenic to human health and the environment.[1,21] Accordingly, Table 1 describes acid, basic, reactive, nitro, vat, disperse, azo, mordant dyes, *etc.*

3. Existing treatment processes for the remediation of dyes

Previously, conventional treatment processes were employed using proper regulatory guidelines for the treatment of dyes in wastewater.[91] However, advanced dye removal processes have been established considering the discharge limit. They include several biological (*e.g.*, ASP, MBR, SBR, MBBR, and CW), coagulation/flocculation, and advanced physicochemical processes (such as adsorption, filtration, photocatalysis, Fenton reaction, ozonation, UV/H_2O_2, and anodic oxidation) reported for the purification of dye-contaminated wastewater.[29,36,92–95] Biological processes use attached and suspended growth systems for the removal of dyes using aerobic and anaerobic or facultative bacteria.[96] In the coagulation/flocculation process, various coagulants are employed to destabilize the charged suspended and colloidal impurities.[32] The advanced physicochemical processes are based on the principle of the sieving process, solid–liquid separation, attraction–repulsion, free radical reactions, catalytic oxidation, and electrochemical reactions. Adsorption is another simple facile process extensively used in the treatment of industrial dye effluents. This process involves the movement of dye molecules present in the liquid phase to a solid surface of various adsorbents.[26,36] Membrane processes such as reverse osmosis (RO), nanofiltration (NF), and microfiltration (MF) have also been successfully employed in the treatment of dye–laden water (more than or about 90% removal efficiency). However, pore blockage and membrane fouling during these processes are still major drawbacks.[93,97–99] In AOPs, active radicals are generated, mainly hydroxyl radicals, which play an important role in degrading persistent dye compounds. However, the high cost/energy requirements and the formation of toxic by-products are a few major constraints in their practical application.[35,100]

In addition, biological processes, such as ASP, MBR, SBR, and MBBR, have shown good efficacy for dye removal. However, the good removal efficiency of dyes by biological processes is overshadowed by their limitations such as space requirements, low removal rate, and inefficiency to treat recalcitrant dye components. The number of articles published on various existing physicochemical and biological processes are compared and shown in Fig. 3a, which presents that adsorption is the most studied process for dye removal. Overall, it can be inferred that in comparison to the existing advanced oxidation, filtration, and biological treatment processes, the adsorption process is beneficial for treating dye wastewater owing to its easy operation, low cost, high efficiency, recycling of the adsorbents, suitability for the treatment of persistent dye compounds and applicability.[40,101]

4. Overview of various adsorbents for the removal of dyes

At present, various adsorbents such as bio-sorbents, carbon-based nano-adsorbents, transition metal-based oxides, MOFs, and polymer-based adsorbents are used to treat dye-containing wastewater. The pie-chart in Fig. 3b displays the percentage of the literature available on dye removal using various adsorbents, where it can be observed that adsorbents such as polymer-based materials and activated carbon are studied more for the removal of dyes.

The possible responsible mechanisms (*i.e.*, surface complexation, electrostatic interaction, and van der Waals force) and processes (*i.e.*, surface diffusion and intraparticle pore diffusion) for the adsorption of dyes are discussed and shown in Tables 2–7. The detection wavelengths for the targeted dyes in the reported studies are also mentioned in Tables 2–7, which may be helpful for readers to measure the concentrations of these dyes. In the following sections, the above-mentioned adsorbents are discussed in detail. The classes of dye molecules, their ecotoxic effects, adsorptive removal of dyes using various classes of adsorbents together with their sub-categories, the critical influencing factors, and responsible adsorption mechanisms are displayed as a flow chart in Fig. 4.

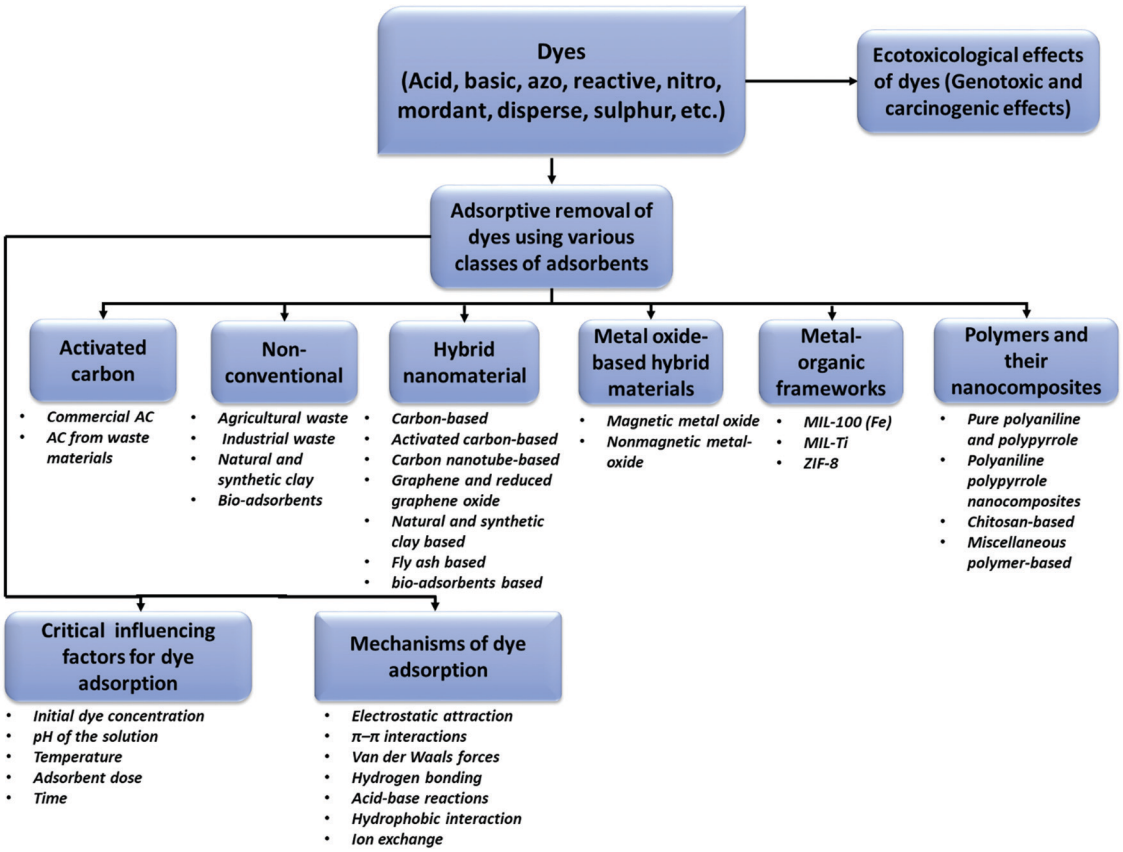

Fig. 4 Flow chart showing the classes of dye molecules, their ecotoxic effects, removal using different classes of adsorbents together with their sub-categories, critical influencing factors, and probable adsorption mechanisms.

4.1. Activated carbon

Activated carbon-based adsorbents are widely studied in the field of adsorption owing to their robust chemical stability, low density, structural diversity, and suitability for field-scale applications. These unique characteristics generally originate from their internal pore morphology, surface characteristics, porosity, pore volume, chemical structure, and presence of functional groups from their source material, including their activation.[102–104] The commercial activated carbon and activated carbon synthesized from various waste materials are discussed in the subsequent section.

4.1.1 Commercial activated carbon. Researchers have reported the use of various commercial activated carbons as adsorbents for the separation of different dyes from wastewater.[62,105,106] For instance, Malik (2004) developed an effective carbon-based adsorbent from mahogany sawdust and directly applied it to adsorb dyes. The experimental data well correlated with the Langmuir model, exhibiting an adsorption capacity of 518 and 327.9 mg g^{-1} for Direct Blue 2B and Direct Green B dyes, respectively.[105] In another study, Mohammadi *et al.* reported the removal of an anionic dye (*i.e.*, MO) using mesoporous carbon CMK-3 (*i.e.*, carbon material kinetic-3) as an adsorbent and observed the extraction of the dye within 60 min. Further, their studies indicated that acidic media facilitated the removal of the dye more than basic media. An increase in the initial dye concentration also has a positive effect on the adsorption capacity. The analyzed equilibrium data well fitted the Langmuir isotherm, following monolayer adsorption (adsorption capacity at 25 °C: 294.1 mg g^{-1}).[62] In another study, Djilani *et al.* used activated carbon prepared from apricot stones and achieved an adsorption capacity of 36.68 and 32.25 mg g^{-1} for MB and MO at a pH of 4.85 and 4.87, respectively. The corresponding adsorption data was found to be well correlated with the Langmuir isotherm.[106] In another study, Rahman (2021) used activated carbon synthesized from red oak (*i.e.*, *Quercus rubra*) for the adsorption of MB and observed adsorption efficiency of 97.18%.[107] According to Giannakoudakis *et al.*, the adsorption of Reactive Black 5 dye on the three different forms of commercials activated carbon, namely, Norit Darco 12 × 20 (DARCO), Norit R008 (R008), and Norit PK 1-3 (PK13) followed the Langmuir, Freundlich, and Langmuir–Freundlich models, achieving an adsorption capacity of 348, 527, and 394 mg g^{-1} in 24 h by the corresponding commercial activated carbon as adsorbents, respectively.[108] Activated carbon was also produced from spent tea leaves (STAC) to remove malachite green (MG), which showed an adsorption capacity of 256.4 mg g^{-1} at 45 °C. These studies showed an increment in the adsorption of MG from aqueous solution up to pH 4 and then became more or less unaltered at higher pH.[109]

4.1.2 Activated carbon from waste materials. Different waste materials such as lemongrass leaf, rice husk, orange peel, and spent tea leaves have been reported as important sources for deriving activated carbon, which can be effectively applied as adsorbents in dye remediation.[110–114] For example, Ahmad *et al.* utilized lemongrass leaf-based activated carbon to remediate methyl red from contaminated water. Their findings showed an optimum dye adsorption capacity of 76.923 mg g^{-1} at pH 2 within 5 h. An increase in the adsorption rate of methyl red dye was mainly observed with an increase in temperature, dye concentration, and contact time. Their thermodynamic study indicated that the adsorption of methyl red dye is endothermic and follows a physisorption process.[110] In addition, Ding *et al.* treated rhodamine B using activated carbon obtained from treated rice husk and achieved its equilibrium removal (478.5 mg g^{-1}) within 5 h. The initial solution pH was found to have an insignificant effect on the adsorption of rhodamine B on the activated carbon.[111] In another work, Lam *et al.* reported an adsorption capacity of 28.5 mg g^{-1} while investigating the adsorption of MG cationic dye using activated carbon prepared from orange peel.[112]

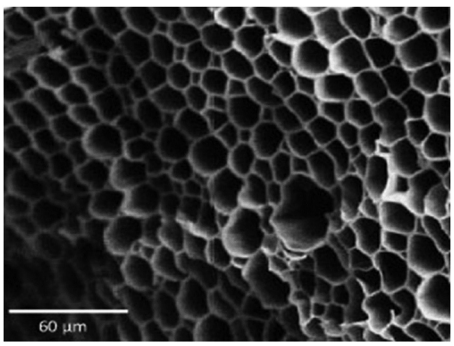

Fig. 5 Morphological image of chemical activated carbon (ACC) prepared from jute sticks [Reprinted with permission from ref. 116. Copyright 2010, Elsevier].

Jawad *et al.* prepared sulfuric acid-treated activated carbon derived from coconut leaves, exhibiting rough and irregular surfaces along with cavities, which was found to be a very effective adsorbent for MB dye (adsorption capacity: 149.3 mg g^{-1}). It is also found that the adsorption capacity increased with an increase in the initial concentration of MB.[115] In another study, chemical activated carbon (ACC) prepared from jute sticks (morphological image is shown in Fig. 5) showed an adsorption capacity of 480 mg g^{-1} for brilliant green dye.[116] Guava leaf-based activated carbon exhibited a maximum adsorption capacity of 39.7 mg g^{-1} to remove CR dye.[117] Low-cost activated carbon derived from Brazilian agriculture waste was also used for the adsorption of dyes, including Basic Blue 26, Basic Green 1, Basic Yellow 2, and Basic Red 1, which exhibited an adsorption capacity in the range of 10–76 mg g^{-1}, 26–83 mg g^{-1}, 27–83 mg g^{-1}, and 21–70 mg g^{-1}, respectively.[118] The adsorption performance of commercial activated carbon and activated carbon derived from various waste materials for the treatment of dye-contaminated water is presented in Table 2.

Table 2 Activated carbon (AC) as an adsorbent in dye removal

Source of AC	Dyes	Experimental conditions	Adsorption capacity/ removal efficiency	Adsorption kinetics; isotherm; and mechanisms
Commercial activated carbon				
Saw-dust[105]	Direct Blue 2B and Direct Green B	Time: 120 min pH: 3	518 and 327.9 mg g^{-1}, respectively	Pseudo-second-order kinetics; Langmuir isotherm model; chemisorption
Apricot stones and commercial activated carbon[106]	Methylene blue (MB) and methyl orange (MO)	C_0: 10 mg L^{-1} T: 298 K Dose: 0.5 g/50 mL pH: 4.85 (MB) and 4.87 (MO) Time: 60–180 min λ_{max}: 665 and 465 nm, respectively	Activated carbon prepared from apricot stones (ASAC): 36.68 and 32.25 mg g^{-1}, respectively. Commercial activated carbon (CAC): 199.60 mg g^{-1} and 35.43 mg g^{-1}, respectively.	Pseudo-second-order kinetics; Langmuir isotherm; chemisorption and intraparticle diffusion
Mesoporous carbon material[62]	MO	Time: 60 min C_0: 1000 mg L^{-1} Dose: 50 mg in 25 mL pH: 3–9 λ_{max}: 465 nm	294.1 mg g^{-1}	Pseudo-second-order kinetics; Langmuir isotherm; chemisorption
Red Oak (*Quercus rubra*)[107]	MB	C_0: 10 mg L^{-1} Dose: 0.25 g/50 mL pH: 10 T: 318 K Agitation speed: 175 rpm Time: 2 h λ_{max}: 660 nm	97.18%	—

Table 2 (*continued*)

Source of AC	Dyes	Experimental conditions	Adsorption capacity/ removal efficiency	Adsorption kinetics; isotherm; and mechanisms
Norit Darco 12 × 20 (DARCO), Norit R008 (R008), and Norit PK 1-3 (PK13)[108]	Reactive Black 5	pH: 10 Dose: 1 g L^{-1} C_0: 500 mg L^{-1} Time: 24 h λ_{max}: 603 nm	348, 527, and 394 mg g^{-1}, respectively	Pseudo-second-order kinetics; Langmuir or Langmuir–Freundlich model; intraparticle diffusion
Activated carbon from waste materials				
Lemongrass leaf[110]	Methyl red	pH: 2 Time: 5 h λ_{max}: 520 nm	76.923 mg g^{-1}	Pseudo-first-order kinetics; Koble–Corrigan isotherm (R^2: 0.997); physisorption
Rice husk[111]	Rhodamine B (RhB)	Time: 5 h pH < 3.20 *T*: 303 K λ_{max}: 554 nm	478.5 mg g^{-1}	Pseudo-second-order kinetics; Langmuir isotherm; chemisorption
Orange peel[112]	Malachite green (MG)	C_0: 1 mg mL^{-1} λ_{max}: 617 nm	28.5 mg g^{-1}	—
Coconut leaves[115]	MB	C_0: 30–400 mg L^{-1} pH: 3–11	149.3 mg g^{-1}	Pseudo-second-order kinetics; Langmuir isotherm; physisorption
Guava leaf[117]	Congo red (CR)	C_0: 10–50 mg L^{-1} λ_{max}: 497 nm	39.70 mg g^{-1}	Pseudo-second-order kinetics; Freundlich isotherm; multilayer adsorption
Brazilian low-cost agriculture waste[118]	Basic Blue 26, Basic Green 1, Basic Yellow 2, and Basic Red 1	C_0: 250 mg L^{-1} Dose: 0.3 g in 100 mL Time: 24 h λ_{max}: 618 nm, 625 nm, 433 nm, and 530 nm, respectively	10–76, 26–83, 27–83, and 21–70 mg g^{-1}, respectively.	Electrostatic interactions
Spent tea leaves[109]	MG	C_0: 220 mg L^{-1} Dose: 0.02 g/25 mL Time: 180 min λ_{max}: 617 nm	256.4 mg g^{-1}	Pseudo-second-order kinetics; Langmuir isotherm; chemisorption
Lemon peels/sodium alginate[119]	MB	C_0: 25 – 300 mg L^{-1} λ_{max}: 664 nm	841.37 mg g^{-1}	Pseudo-first-order and pseudo-second-order kinetics; Langmuir isotherm; electrostatic interaction and external surface adsorption

C_0: initial dye concentration; *T*: temperature; and λ_{max}: maximum wavelength detected for the analysis of dye.

4.2. Non-conventional adsorbents

In recent years, several non-conventional adsorbents have been gaining substantial attention as potential economic alternatives of costly adsorbent materials to remove toxic pollutants.[120] This includes the utilization of abundantly available agricultural, industrial, natural resources, bio wastes, *etc.* as waste materials. These waste materials prior to their application as adsorbents are subjected to various processes such as chemical treatment, conversion to powder form, and decomposition.[60,121–123] Considering this, different waste materials to adsorb toxic dyes from contaminated water are described below.

4.2.1 Agricultural waste materials. Agricultural waste materials, such as raw maize cob, exhausted coffee ground powder, saw-dust, black cumin, neem leaf, pineapple leaf, and pine tree leaves, have been used by many researchers in dye remediation of contaminated water.[60,121–125] Abubakar and Ibrahim (2019) used raw maize cob for the adsorption of bromophenol blue (96.5%) and bromothymol blue (94.4%) present in wastewater at the equilibrium time of 125 and 110 minutes, respectively. The effect of increasing the initial dye concentration on dye adsorption showed positive effects, and the dye adsorption followed the Temkin isotherm model.[122] In another work, the adsorption of rhodamine B and rhodamine 6G on exhausted coffee ground powder achieved an adsorption capacity of up to 5.3 and 17.4 μmol g^{-1}, respectively.[60] It was proposed that electrostatic, hydrophobic, and intermolecular interactions account for the adsorption of Rhodamine dye onto the adsorbent surface (Fig. 6). Sodium hydroxide-treated sawdust exhibited an adsorption

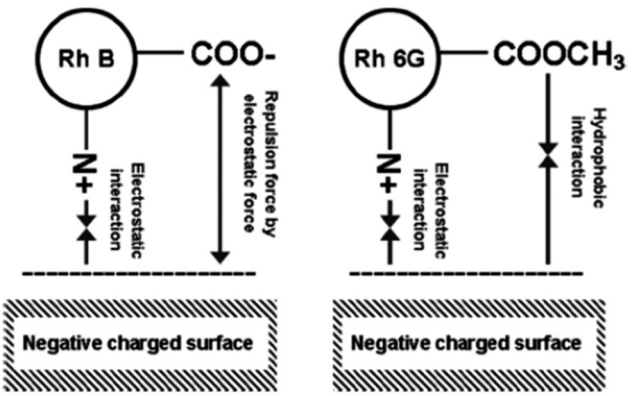

Fig. 6 Possible adsorption mechanisms on the surface of exhausted coffee ground powder [Reprinted with permission from ref. 60. Copyright 2017, Elsevier].

capacity of 55.86 mg g^{-1} for brilliant green dye in 3 h.[121] In a study by Siddiqui *et al.*, an antimicrobial *Nigella sativa* seed-based manganese dioxide/black cumin (MnO_2/BC) nanocomposite was used for the adsorption of MB (adsorption capacity: 185.19 mg g^{-1} at pH 7.0 and 318 K). The process of adsorption was endothermic and best described by the Langmuir isotherm. The adsorption mechanism involved hydrogen bonding and electrostatic interactions of MB onto the surface of MnO_2/BC.[123] Pineapple leaf powder,[125] pine tree leaves,[126] and *Platanus orientalis* leaf powder[127] as adsorbents achieved the maximum removal capacities of 48.72, 71.94, and 114.94 mg g^{-1}, corresponding to the contact time of 150, 120, and 70 min in the removal of Basic green 4, Basic red 46, and MB dye, respectively. Neem leaf powder was also used for the adsorption of brilliant green dye,[124] which showed 0.554 mmol g^{-1} adsorption capacity within 240 min. Microwave-assisted spent tea leaves exhibited a maximum adsorption capacity of 242.72 mg g^{-1} for Eriochrome black-T adsorption in a contact time of 24 h.[113]

4.2.2 Industrial waste materials. Various industrial wastes, including fly ash, slurry, and ceramic wastes, have been regularly used as adsorbents for dye removal from contaminated water.[128–131] Jain *et al.* used steel and fertilizer industrial waste as an adsorbent material for the adsorption of ethyl orange, metanil yellow, and Acid Blue 113 dyes. In this process, they achieved an adsorption capacity of 198, 211, and 219 mg g^{-1}, respectively.[128] Coal fly ash exhibited maximum removal efficiencies of more than 90% and up to 85% in 24 h for MB and crystal violet dyes, respectively.[129] Bhatnagar and Jain (2005) used carbonaceous slurry waste as an adsorbent to remove RhB and Bismark Brown R dye. They achieved an adsorption capacity of 91.1 and 85 mg g^{-1} at a contact time of nearly 25 min for RhB and Bismarck Brown R dye, respectively.[130] Ceramic adsorbents derived from industrial waste coal gangue achieved an adsorption capacity of 1.044 and 2.170 mg g^{-1} for Cationic Red X-5GN and Cationic Blue X-GRRL dyes at a contact time of 180 min, respectively.[131] The possible mechanisms displayed in Fig. 7 suggest electrostatic attraction, H-bonding, *etc.*, playing an essential role in the adsorption of the X-5GN and X-GRRL dyes. Furthermore, industrial waste shells of eggs showed an adsorption capacity of 94.9 and 49.5 mg g^{-1} in removing MB and CR, respectively.[132]

4.2.3 Natural and synthetic clay. The easy availability, low cost, high porosity, high potential for ion exchange, and non-toxicity of several natural and synthetic clays have resulted in their significant use as adsorbents for dye removal from aqueous solution.[133–136] For example, sulfuric acid-treated coal bearing kaolinite achieved a maximum adsorption capacity of MB dye corresponding to 101.5 mg g^{-1}.[133] In another work, the adsorptive behavior of RhB on sodium montmorillonite clay showed an adsorption capacity of 42.19 mg g^{-1}.[137] The adsorption process involved electrostatic attraction between the negatively charged adsorbent surfaces and positively charged cationic dye. Santos and Boaventura (2008) used sepiolite to remove Basic Red 46 and Direct Blue 85 dyes, achieving an adsorption capacity of 108 and 454 mg g^{-1}, respectively.[134] Acid-treated palygorskite was employed to remove crystal violet, cationic light yellow (7GL), MB, and MO dyes, exhibiting adsorption capacities of 223.43, 290.86, 86.53, and 276.11 mg g^{-1}, respectively.[136] Palygorskite modified by 3-aminopropyl triethoxysilane was successfully employed to remove reactive red 3BS, reactive blue KE-R, and reactive black GR dyes in 20 min with adsorption capacities of 34.23, 38.59, and 60.13 mg g^{-1}, respectively.[135] Kismir and Aroguz (2011) reported an adsorption capacity of 1.18 mg g^{-1} for the adsorption of brilliant green dye on Saklikent mud as an adsorbent.[138] Flower-like[139] and hollow LDH[140] exhibited an adsorption capacity of 500.6 and 210 mg g^{-1} in less than 10 min for methyl orange, respectively.

4.2.4 Bio-adsorbents. Significant advancement has been made in the field of dye removal from polluted water using biosorbents, such as *Spirulina platensis*, *Penaeus indicus* shrimp, cellulose, *Ganoderma lucidum*, wheat flour, and Graham flour.[141–146] According to Dotto *et al.*, Acid Blue 9 and FD&C Red No. 40 were effectively adsorbed on the biosorbent synthesized from *Spirulina platensis*. The scanning electron microscopy (SEM) image of the *Spirulina platensis* biomass in Fig. 8 shows the presence of pores and cylindrical filaments on its surface, revealing the adsorption capability of *Spirulina platensis*. The experimental analysis showed a biosorption capacity of 400.3 and 1653.0 mg g^{-1} for FD&C Red No. 40 and Acid Blue 9 dye, respectively, at initial solution pH of 2 and contact time of 100 min.[141] The shell of *Penaeus indicus* shrimp was also found to be an effective adsorbent

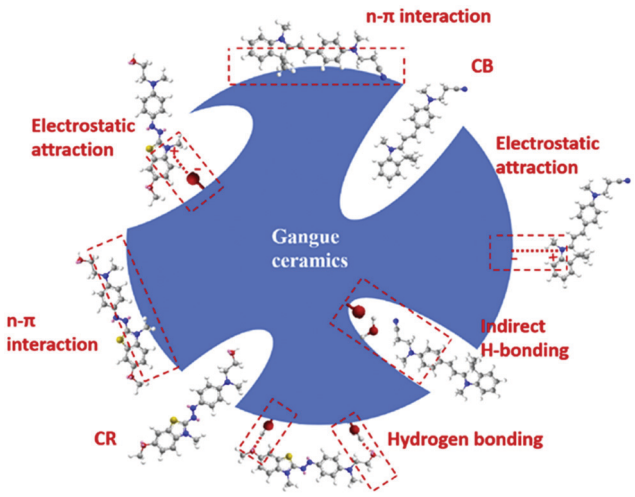

Fig. 7 Possible adsorption mechanisms of adsorption of cationic dyes by gangue ceramics [Reprinted with permission from ref. 131. Copyright 2019, Elsevier].

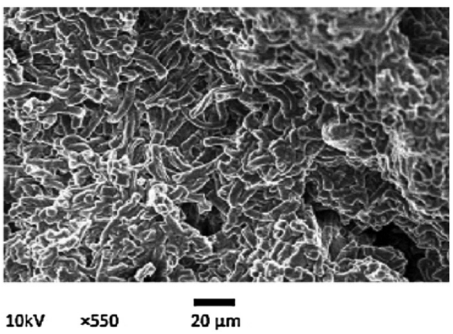

Fig. 8 Scanning electron microscopy image of *Spirulina platensis* biomass [Reprinted with permission from ref. 141. Copyright 2012 Elsevier].

for Acid Blue 25, and dye biosorption fitted well with the pseudo-second-order model.[142] The optimum condition of this dye adsorption corresponds to pH 2 and 0.1 g L^{-1} dose, resulting in an adsorption capacity of 1093 mg g^{-1}. The adsorption capacities of 2.197, 2.120, 2.038, and 1.480 mg g^{-1} were achieved on neem sawdust for the removal of crystal violet, MB, MG, and RhB dyes, respectively, from contaminated water in 30 min.[147] The adsorption capacities of 1201 and 1070 mg g^{-1} were observed within 3 h on cellulose nanocrystal-reinforced keratin for the adsorption of Reactive Black 5 and Direct Red 80, respectively.[143] The adsorption process of both the dyes was well correlated with the Langmuir isotherm. Wu *et al.* used the spent substrate of *Ganoderma lucidum* for removing MG, safranine T, and MB dyes and observed the adsorption capacities of 40.65, 33, and 22.37 mg g^{-1}, respectively, in 4 h.[144] The adsorption performances of various non-conventional adsorbents are listed in Table 3.

Table 3 Non-conventional adsorbents in dye removal

Examples of adsorbents	Dyes	Experimental conditions	Adsorption capacity/ removal efficiency	Adsorption kinetics; isotherm; and mechanisms
Waste materials from agricultural				
Raw maize cob[122]	Bromophenol blue and bromothymol blue	C_0: 10–100 mg L^{-1} Dose: 0.5–4.0 g Time: 125 and 110 min, respectively λ_{max}: 591.22 and 430.9 nm, respectively	96.53%, and 94.39%, respectively	Pseudo-second-order kinetics; Temkin isotherm; chemisorption
Exhausted coffee ground powder[60]	Rhodamine (Rh) dye (Rh B and Rh 6G)	Dose: 50 mg/50 mL Time: 3 h λ_{max}: 554 and 526 nm, respectively	5.255 and 17.369 μmol g^{-1}	Pseudo-first-order kinetics and pseudo-second-order kinetics; Langmuir isotherm; chemisorption
NaOH treated saw dust[121]	Brilliant green	Time: 3 h Dose: 4 g L^{-1} C_0: 100 mg L^{-1} T: 303 K	55.86 mg g^{-1}	Pseudo-second-order kinetics; Temkin and Redlich–Peterson isotherm; physisorption and boundary layer diffusion
Nigella sativa seed-based nanocomposite-MnO_2/BC[123]	MB	Dose: 1.0 g L^{-1} C_0: 10 mg L^{-1} λ_{max}: 660 nm	185.185 mg g^{-1}	Pseudo-second-order kinetics; Freundlich isotherm; intraparticle diffusion, and film diffusion action
Neem leaf powder[124]	Brilliant green	C_0: 10–50 mg/dm^3 Time: 4 h T: 300 K λ_{max}: 624 nm	0.149 to 0.554 mmol g^{-1}	First-order kinetics; Langmuir isotherm; external surface and pore diffusion
Pineapple leaf[125]	Basic green 4 (BG4)	C_0: 50 mg L^{-1} pH: 9.0 Time: 150 min Dose: 5 g L^{-1} T: 298 K λ_{max}: 618 nm	48.72 mg g^{-1}	Pseudo-second-order kinetics; Langmuir isotherm; chemisorption
Pine tree leaves[126]	Basic Red 46 (BR 46)	C_0: 20–100 mg L^{-1} Dose: 1–6 g L^{-1} T: 298–318 K Time: 0–120 min λ_{max}: 530 nm	71.94 mg g^{-1}	Pseudo-second-order kinetics; Langmuir isotherm; physisorption
Platanusorientalis leaf[127]	MB	C_0: 20–180 mg L^{-1} Dose: 80 mg/50 mL T: 25–60 °C Time: 0–70 min λ_{max}: 664 nm	114.94 mg g^{-1}	Pseudo-second-order kinetics; Langmuir isotherm; endothermic adsorption
Microwave-assisted spent black tea leaves[113]	Eriochrome black T (EBT)	C_0: 10–400 mg L^{-1} Dose: 0.25–5.0 g L^{-1} T: 298–338 K Time: 24 h λ_{max}: 518 nm	242.72 mg g^{-1}	Pseudo-second-order kinetics; Langmuir isotherm; physico-chemical interaction
Rice husk[148]	MB	C_0: 100 mg L^{-1} Dose: 250 mg L^{-1} pH: 10 T: 298 K λ_{max}: 664 nm	1350 mg g^{-1}	Pseudo-first-order kinetics; Freundlich and Sips isotherm; electrostatic interaction
Waste materials from industry				
Steel and fertilizer industries wastes[128]	Ethyl orange, metanil yellow, and Acid Blue 113	Time: 3 h pH: 7 ± 0.5 λ_{max}: 475 nm, 432 nm, and 532 nm, respectively	198 mg g^{-1}, 211 mg g^{-1}, and 219 mg g^{-1}, respectively	Pseudo-first-order kinetics; Langmuir isotherm; physisorption
Coal fly ash[129]	MB and crystal violet (CV)	Dose: 0.08 g L^{-1} Time: 24 h λ_{max}: 665 nm and 590 nm, respectively	CV: >90% MB: <85%	Pseudo-second-order kinetics; Langmuir isotherm; endothermic adsorption for CV and exothermic reaction for MB dye.

Table 3 (*continued*)

Examples of adsorbents	Dyes	Experimental conditions	Adsorption capacity/ removal efficiency	Adsorption kinetics; isotherm; and mechanisms
Amine-functionalized biomass fly ash[149]	Alizarin red S (ARS) and bromothymol blue (BTB)	Time: 10 min and 5 min, respectively λ_{max}: 422 nm and 432 nm, respectively	13.42 and 15.44 mg g^{-1}, respectively	Linear pseudo-second-order kinetics; modified Langmuir–Freundlich isotherm; electrostatic interaction
Carbonaceous slurry waste[130]	RhB and Bismark Brown R	pH: 5.5–6.5 Time: ~25 min λ_{max}: 554 nm and 460 nm, respectively	91.1 mg g^{-1} and 85 mg g^{-1}, respectively	First-order and pore-diffusion; Langmuir isotherm; physisorption
Industrial waste coal gangue[131]	Cationic Red X-5GN (CR) and Cationic Blue X-GRRL (CB)	Time: 3 h pH: 2–12	1.044 mg g^{-1} and 2.170 mg g^{-1}, respectively	Pseudo-second-order and Elovich kinetics; Freundlich isotherm for CR and Langmuir isotherm for CB dye; electrostatic attraction, n–π interactions, and hydrogen bonding
Industrial waste shells of egg[132]	MB and CR	C_0: 50–1000 mg L^{-1} T: room temperature Time: 10–120 min	94.9 mg g^{-1} and 49.5 mg g^{-1}, respectively	Pseudo-second-order kinetics; Freundlich isotherm; Electrical double layer mechanism, and electrostatic attraction for MB and CR dye, respectively
Natural and synthetic materials				
Green clay minerals[150]	MB	Time: 60 min 300 rpm Dose: 200 mg/250 mL T: 293 K λ_{max}: 665 nm	241.96 mg g^{-1}	Langmuir isotherm; single-layer adsorption
Natural clay[151]	Basic Red 46	Dose: 10 mg/100 mL pH: 7 λ_{max}: 530 nm	594 mg g^{-1}	Pseudo-second-order kinetics; Langmuir isotherm; electrostatic interactions, including hydrogen bonding
Sodium montmorillonite[137]	RhB	pH: 7 λ_{max}: 554 nm	42.19 mg g^{-1}	Pseudo-second-order kinetics; Langmuir isotherm; high electrostatic attraction
Sepiolite[134]	Astrazon Red (Basic Red 46) and Sirius Blue (Direct Blue 85)	C_0: 75 mg L^{-1} and 150 mg L^{-1}, respectively pH: 8 and 3.5, respectively T: 313 K and 303 K, respectively. λ_{max}: 525 nm and 590 nm, respectively	108 mg g^{-1} and 454 mg g^{-1}, respectively	Langmuir isotherm and Freundlich isotherm; physisorption
Acid-treated palygorskite[136]	Crystal violet (CV), cationic light yellow (7GL), MB, and MO	C_0: CV, 7GL, MB, and MO, were 500, 500, 200, 500, and 200 mg dm^{-3}, respectively. λ_{max}: 581, 415, 662, 463, and 642 nm, respectively	CV: 223.43 mg g^{-1} 7GL: 290.86 mg g^{-1} MB: 86.53 mg g^{-1} MO: 276.11 mg g^{-1}	Sips and Langmuir isotherm; bridging effect mechanism
Palygorskite modified by 3-aminopropyl triethoxysilane[135]	Reactive red 3BS, reactive blue KE-R, and reactive black GR	Time: 20 min C_0: 20–600 mg L^{-1} pH: 2–12 λ_{max}: 546 nm, 620 nm, and 602 nm, respectively	34.23 mg g^{-1}, 38.59 mg g^{-1}, and 60.13 mg g^{-1}, respectively	Pseudo-second-order kinetics; Langmuir isotherm; electrostatic attraction
Saklikent mud[138]	Brilliant green	C_0: 1–20 mg L^{-1} Dose: 0.1 g/50 mL λ_{max}: 625 nm	1.18 mg g^{-1}	Pseudo-first-order kinetics and intra-particle model at 25 °C and pseudo-second-order kinetics at the higher temperature. Langmuir isotherm; electrostatic attraction
Flower-like LDH[139]	MO	C_0: 100 mg L^{-1} Dose: 1 g pH: 3 T: 298 K Time: 10 min	500.6 mg g^{-1}	Pseudo-second-order kinetics; Langmuir isotherm; chemisorption
Hollow LDH nanowires[140]	MO	C_0: 5–40 mg L^{-1} Dose: 0.5 g L^{-1} Time: 90% removal at <10 min	210 mg g^{-1}	Langmuir isotherm

Table 3 (*continued*)

Examples of adsorbents	Dyes	Experimental conditions	Adsorption capacity/ removal efficiency	Adsorption kinetics; isotherm; and mechanisms
Bio-adsorbents				
Spirulina platensis[141]	Acid blue 9 and FD&C Red No. 40	pH: 2 Agitation speed: 400 rpm and 225 rpm for Acid Blue 9 and FD&C Red No. 40, respectively. Time: 20–100 min λ_{max}: 408 and 500 nm, respectively.	1653.0 mg g^{-1} and 400.3 mg g^{-1}, respectively, 95% for both	Avrami kinetic; electrostatic attraction
Shrimp shell[142]	Acid blue 25	pH: 2 Dose: 0.1–0.4 g L^{-1} Time: 30 min λ_{max}: 600 nm	1093 mg g^{-1}	Pseudo-second-order kinetics; Langmuir, Freundlich and Temkin isotherm; physisorption
Neem sawdust[147]	CV, MB, MG, and RhB	C_0: 6–12 mg L^{-1} Dose: 0.5 g in 100 mL T: 25–45 °C pH: 7.2 Time: 30 min λ_{max}: 592 nm, 664 nm, 616 nm, and 555 nm, respectively	2.197, 2.120, 2.038, 1.480 mg g^{-1}, respectively	
Cellulose nanocrystal-reinforced keratin[143]	Reactive Black 5 and Direct Red 80	C_0: 200 mg L^{-1} Time: 3 h pH: 3 Dose: 0.1 g/200 mL λ_{max}: 595 nm and 543 nm, respectively	1201 mg g^{-1} and 1070 mg g^{-1}, respectively	Pseudo-second-order kinetics; Langmuir isotherm; electrostatic interaction
Spent substrate of *Ganodormalucidum*[144]	MG, safranine T, and MB	C_0: 10–120 mg L^{-1} pH: 6 Time: 4 h λ_{max}: 617 nm, 530 nm, and 664 nm, respectively	40.65 mg g^{-1}, 33 mg g^{-1}, and 22.37 mg g^{-1}, respectively	Pseudo-second-order kinetics; Freundlich isotherm; chemisorption
Carbohydrate polymeric biodegradable adsorbent of wheat flour[145]	Rhodamine B (RhB)	C_0: 5.0 mg L^{-1} pH: 5.5	142.26 mg g^{-1}	Langmuir adsorption; electrostatic interaction, π–π conjugation, and hydrogen bonding conjugation
Wood-based colloidal cellulose nanocrystals[152]	Auramine O (AO)	pH: not adjusted C_0: 2.5–30 mg L^{-1} λ_{max}: 430 nm	20 mg g^{-1}	Pseudo-second-order kinetics; Freundlich isotherm; electrostatic interactions and hydrogen bonding
Egg shell membrane[153]	Basic Fuchsin (BF)	pH: 6 Time: 25 min T: 298 K	48 mg g^{-1}	Pseudo-second-order kinetics; Freundlich isotherm; electrostatic interactions
Arginine-modified starch resin[154]	Acid fuchsin (AF) and Acid Orange G (AOG)	C_0: 0.25 mmol/L Dose: 0.1 g/20 mL Time: 1 h T: 298 K	AF: 21.326 mg g^{-1} AOG: 23.485 mg g^{-1}	Pseudo-second-order kinetics; Langmuir isotherm; electrostatic attractions, prevalent hydrogen bonds, and hydrophobic interactions (van der Waals force)

C_0: initial dye concentration; T: temperature; and λ_{max}: maximum wavelength detected for the analysis of dye.

4.3. Hybrid nanomaterials

Nanomaterials have been extensively used for water treatment applications because of their enhanced surface area and high adsorption-to-mass ratio. Accordingly, the combination of two or more nanomaterials, which is referred to as hybrid nanomaterials, exhibits multi-functionalities found to be very effective to remove dyes from contaminated water, as described below.[155]

4.3.1 Carbon-based hybrid nanocomposite. Carbon-based hybrid nanocomposites are associated with easy synthesis, cost-effectiveness, availability, non-toxicity, high porosity, *etc.*, similar to other carbon-based nanocomposites. Ultrafine nickel/carbon (dose: 2 g L^{-1}) on treatment with RhB and MB showed an adsorption capacity of 5.269 and 7.415 mg g^{-1}, respectively.[156] Manippady *et al.* investigated the adsorption of CR and MB dye onto iron–carbon hybrid magnetic nanosheets and achieved an adsorption capacity of 531.9 and 185.2 mg g^{-1}, respectively, in 24 min.[157] In another study, a porous silicon–carbon–nitrogen (Si–C–N) hybrid was employed to remove methyl blue and acid fuchsin dyes, achieving an adsorption capacity of 1327.7 and 1084.5 mg g^{-1}, respectively.[158] The possible mechanism displayed in Fig. 9 suggests the presence of electrostatic interactions and van der Waals forces between the adsorbent and dye. An Ni/porous carbon nanotube nanocomposite was used to remove MG, CR, RhB, MB, and MO dye, exhibiting adsorption capacities of 898, 818, 395, 312, and 271 mg g^{-1}, respectively.[159]

4.3.2 Activated carbon-based hybrid nanocomposites. Activated carbon-based hybrid nanocomposites have been widely used in the purification of contaminated water. Wang *et al.* observed an adsorption capacity of 416.67 mg g^{-1} (303 K) using

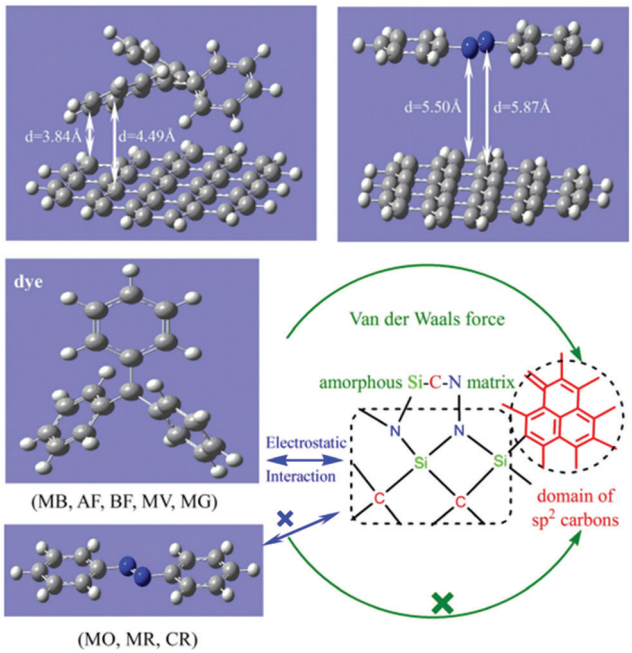

Fig. 9 Adsorption mechanisms for porous Si–C–N hybrid material [Reprinted with permission from ref. 158. Copyright 2015, Nature Research].

activated carbon aerogel immobilized with konjac glucomannan for the removal of MB.[160] In another study, ZnO nanoparticles loaded on *Parthenium* weed activated carbon achieved more than 99% removal of MB in 60 min.[161] The adsorption of RhB and Orange G using sulfonic acid-modified activated carbon resulted in an adsorption capacity of 757.6 and 318.5 mg g^{-1}, respectively.[162] Gong *et al.* used activated carbon synthesized from finger citron residue as a new type of adsorbent for the removal of harmful dyes, namely, anionic dyes such as MO and cationic dyes such as MB, from contaminated water, achieving an adsorption capacity of 934.58 (MO) and 581.40 mg g^{-1} (MB).[163]

4.3.3 Carbon nanotube-based hybrid nanomaterials. Recently, carbon nanotube (CNT)-based nanohybrid materials have receive tremendous attention because of their high specific surface area, small sizes, and hollow structures.[164,165] According to Gong *et al.*, these hybrids are more efficient for the adsorption of organic contaminants compared to even activated carbon.[70] Thus, the unique features of carbon nanotubes have been supplemented in the formation of several nanocomposites for dye removal from contaminated water. CNTs exhibited an adsorption capacity of 44.64 mg g^{-1} for CI Reactive Red 2 dye.[166] Magnetic multi-walled CNT (MMWCNT) exhibited a poor adsorption performance for MB, neutral red, and brilliant cresyl blue dyes.[70] In another study, Yao *et al.* achieved a maximum adsorption capacity of 51.74 mg g^{-1} MO dye on MMWCNT from wastewater.[167] Further, Sui *et al.* studied the adsorption of MB and MO on a synthesized calcium alginate/MWCNT hybrid and reported the maximum adsorption capacity of 606.1 and 12.5 mg g^{-1}, respectively.[168] HNO_3/NaClO/MWCNT nanohybrid[169] and magnetite/MWCNT[170] hybrid materials showed a maximum adsorption capacity of 55 and 48.06 mg g^{-1} for the removal of bromothymol blue and MB dyes, respectively.

4.3.4 Graphene and reduced graphene oxide nanocomposites. Graphene oxide (GO) has been used as an adsorbent for dye removal from wastewater, such as Direct Red 81 and Indosol SFGL direct blue,[171] crystal violet and methyl orange,[172] and methylene blue.[173–176] The adsorption mechanism involves strong interactions between graphene oxide (functionalized with hydroxyl and carboxylic groups) and active functional groups present in the dye.[171,177] In addition, several studies have also been reported on GO and reduced graphene oxide (rGO)-based nanocomposites for the adsorption of dye from contaminated water. Zheng *et al.* prepared a 3D hierarchical GO–NiFe layered double hydroxide (LDH) sandwich hybrid as an adsorbent for the removal of CR and MO dye. Fig. 10 shows that the GO–NiFe-LDH is comprised of a hierarchically well-ordered structure, and both sides of GO is fully protected by ultrathin NiFe-LDH nanosheets, resulting in a sandwich-like architecture. The hybrid exhibited higher adsorption phenomena for CR and MO, as evident from the adsorption capacity values of 489 and 438 mg g^{-1}, respectively. This was ascribed to the presence of electrostatic attraction and ion exchange reactions between the dye molecules and hybrid adsorbents.[178] In another work, graphene/polyaniline (PANI)/Fe_3O_4 was used as a nanoadsorbent for the removal of CR from dye contaminated water.[179] It showed an excellent adsorption performance (adsorption capacity: 248.76 mg g^{-1}) for CR dye. MB dye (initial concentration: 250 mg L^{-1}) on treatment with GO showed an adsorption capacity of about 714 mg g^{-1}.[174] In another work, graphite oxide was used as an adsorbent to separate MB and MG dyes, with maximum adsorption capacities of 351 and 248 mg g^{-1}, respectively.[180] Heidarizad and Şengör (2016) used GO/magnesium oxide nanocomposites for the removal of MB dye and achieved an adsorption capacity of 833 mg g^{-1} in a contact time up to 60 min.[181] Investigations have also been reported using a combination of magnetic Fe_3O_4/carboxylate GO[182] and GO/Fe_3O_4[183] nanostructures as adsorbents in dye removal. It was inferred that GO/Fe_3O_4 and Fe_3O_4/carboxylate GO achieved complete removal (MB) and maximum adsorption capacity of 36 mg g^{-1} (MB) and 22.1 mg g^{-1} (RhB), respectively.

Further, GO-based nanocomposites have been reported for dye removal such as porous core–shell graphene/SiO_2 nanocomposites for the removal of cationic neutral red dye,[184] whereas GO-shielded Mg–Al-LDH,[185] Au nanorod-doped Cu_2O core–shell nanocube-embedded rGO composite,[186] and GO-fabricated Fe–Al

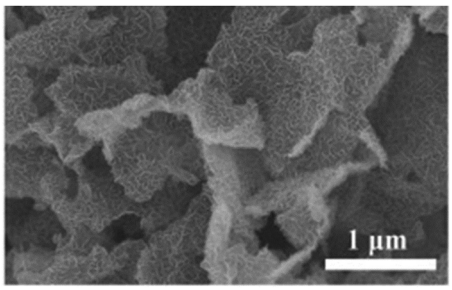

Fig. 10 FE-SEM image of GO–NiFe LDH [Reprinted with permission from ref. 178. Copyright 2019, Elsevier].

bimetal oxide composite[187] were reported for the for removal of MB. Several other GO-based nanocomposites have also been reported to adsorb various classes of dyes, for example, the removal of MB using impregnated graphene in porous wood filters,[188] Fe_3O_4/GO composite,[189] Fe_3O_4 nanoparticle-functionalized GO/g-C_3N_4 nanocomposite,[190] and metal ferrite-enabled GO[191] and PANI–GO–Fe_3O_4 hybrid nanocomposite[192] for the removal of CR and MO.

4.3.5 Hybrids of natural and synthetic clay. Hybrids adsorbents comprised of natural and synthetic clay-based materials possess several advantages, such as low cost, non-toxicity, thermal resistance, porosity, ion exchange ability, and the possibility of modification with various functionalities.[193] Consequently, nanohybrids of natural and synthetic clay have been harnessed as adsorbents to remove dyes from wastewater. According to Marrakchi *et al.*, the maximum adsorption capacity of 40.97 and 190.97 mg g^{-1} was achieved in 30 h on cross-linked chitosan/sepiolite clay for MB and reactive orange, respectively.[194] The removal efficiency of MO dye on an Mg–Al-layered double hydroxide supported MOF exceeded 99% at the onset of 20 min.[195] The adsorptive removal of reactive red, CR, and Acid Red 1on an Mg–Al-layered double hydroxide fitted well with the Langmuir model.[196] The layered double hydroxide nanohybrid (Mg–Al–NO_3) exhibited a maximum adsorption capacity of 0.8, 1.089, and 1.418 mmol g^{-1} for the adsorption of amaranth, diamine green B, and brilliant green dyes, respectively.[197]

4.3.6 Hybrids of fly ash. Fly ash is generally considered a by-product from coal-based industries and is often used either alone or in combination with other materials as a hybrid adsorbent in water purification.[198,199] This is mainly attributed to its high porosity, economic viability, and easy availability.[200] The adsorption study on MB dye using fly ash geopolymer monoliths attained a maximum adsorption capacity of 15.4 mg g^{-1} in 30 h and the absorbent could be reused for up to five cycles.[199] Novais *et al.* reported the adsorption of MB dye on porous biomass fly ash-based geopolymer spheres. The findings showed an adsorption capacity of 79.7 mg g^{-1} in 30 h and reusability for up to eight cycles.[198] Further, Duta and Visa (2015) conducted a study on the adsorption of a mixture of bemacid red and bemacid blue dye on fly ash–TiO_2 and noted the adsorption capacity of 4.0 and 1.2 mg g^{-1}, respectively.[201] In another study, a maximum adsorption capacity of 24.8 mg g^{-1} was reported for the adsorption of Orange II dye on $Ca(OH)_2$/Na_2FeO_4 modified fly ash.[202]

4.3.7 Hybrids of bio-adsorbents. Bio-adsorbents can be easily modified and blended with other components, making them suitable as adsorbents for the removal of dyes from contaminated water. Cross-linked beads of an activated oil palm ash zeolite/chitosan composite showed an adsorption capacity of 199.2 and 270.27 mg g^{-1} for MB and acid blue dye, respectively.[203] Liu *et al.* reported that cellulose-*g*-poly(acrylic acid-*co*-acrylamide) exhibited an adsorption capacity of 1602 and 1814 mg g^{-1} for of Acid Blue 93 and MB dye, respectively.[204] A sulphonated bio-adsorbent from waste hawthorn kernel as adsorbent attained a maximum adsorption capacity of 151.5 mg g^{-1} for MB dye with a contact time of up to 6 h.[205] In another work, an adsorption study was conducted for the removal of MB dye on agricultural waste/GO.[206] This study revealed a maximum adsorption capacity of 414.03 mg g^{-1} (pH = 12) with the successful reuse of the adsorbent for up to five cycles. Further, the dye adsorption was well correlated with the Temkin isotherm. The performance of various hybrid materials as adsorbents for the treatment of dyes is presented in Table 4.

Table 4 Hybrid nanomaterial as adsorbents for dye removal

Adsorbent	Dyes	Experimental conditions	Adsorption capacity/ removal efficiency	Adsorption kinetics, isotherm, and mechanisms
Carbon-based hybrid nanocomposite				
Ultrafine Ni/C[156]	RhB and MB	Dose: 2 g L^{-1} C_0: 5 mg L^{-1} Time: 2 h λ_{max}: 554 and 664 nm, respectively	5.269 and 7.415 mg g^{-1}, respectively	Pseudo-second-order kinetics; Freundlich isotherm; chemisorption process
Iron–carbon hybrid magnetic nanosheets[157]	CR and MB	Time: 24 min pH: 2 and 8, respectively Dose: 6 mg/15 mL λ_{max}: 662 and 664 nm, respectively.	531.9 and 185.2 mg g^{-1}, respectively	Pseudo-second-order kinetics; Langmuir isotherm; chemisorption
Hierarchically porous silicon–carbon–nitrogen hybrid materials[158]	Methyl blue and acid fuchsin	C_0: 300 mg L^{-1} and 200 mg L^{-1}, respectively	1327.7 mg g^{-1} and 1084.5 mg g^{-1} respectively	Pseudo-second-order kinetics; Langmuir isotherm; Chemisorption
Ni/porous carbon-CNT[159]	MG, CR, RhB, MB, and MO	C_0: 20 mg L^{-1} Time: 60 min	898 mg g^{-1}, 818 mg g^{-1}, 395 mg g^{-1}, 312 mg g^{-1}, and 271 mg g^{-1}, respectively	Pseudo-second-order kinetics; Langmuir isotherm; multilayer adsorption mechanism
Activated carbon-based hybrid nanocomposites				
Konjac glucomannan/ activated carbon aerogel[160]	MB	C_0: 140 mg L^{-1} Dose: 10 mg/20 mL T: 313 K	416.67 mg g^{-1}	Pseudo-second-order kinetics; Langmuir isotherm; density gradient force and hydrogen bond interaction

Table 4 (*continued*)

Adsorbent	Dyes	Experimental conditions	Adsorption capacity/ removal efficiency	Adsorption kinetics, isotherm, and mechanisms
ZnO-NP-loaded *Parthenium* weed activated carbon (ZnONPs-PWAC)[161]	MB	C_0: 100 mg L^{-1} pH: 6 Dose: 50 mg/100 mL Time: 60 min λ_{max}: 670 nm	~99%	—
Sulfonic acid-modified activated carbon (MTLAC-SA) and MTLAC[162]	RhB and Orange G	C_0: 200–800 mg L^{-1} λ_{max}: 664 nm and 476 nm, respectively	757.6 mg g^{-1} using MTLAC-SA and 318.5 mg g^{-1} using MTLAC, respectively	Pseudo-second-order kinetics; Langmuir isotherm; homogeneous adsorption
Finger-citron-residue-based activated carbon[163]	MO and MB	C_0: 50–500 mg L^{-1} λ_{max}: 464 nm and 664 nm, respectively	934.58 and 581.40 mg g^{-1}, respectively	Pseudo-second-order kinetics; Langmuir isotherm; π–π stacking interaction and electrostatic attraction
Carbon nanotubes[166]	Procion Red MX-5B (CI reactive red 2)	Dose: < 0.25 g L^{-1} pH: 6.5 T: 291 K λ_{max}: 538 nm	44.64 mg g^{-1}	Pseudo-second-order kinetics; Langmuir isotherm; physisorption
Calcium alginate/multi-walled carbon nanotubes[168]	MB and MO	pH: 4–12 for MB and <2 for MO	606.1 and 12.5 mg g^{-1}, respectively	Pseudo-second-order kinetics; Langmuir isotherm; Opposite charge attraction
Magnetic multi-wall carbon nanotube[70]	MB, neutral red, and brilliant cresyl blue	C_0: 1.4–37.4 mg L^{-1} Dose: 0.5 g L^{-1} pH: ~7	15.74 mg g^{-1}, 20.33 mg g^{-1}, and 23.55 mg g^{-1}, respectively	Pseudo-second-order kinetics; Freundlich isotherm; van der Waals interactions occurring
Multi-wall carbon nanotubes[167]	MO	C_0: 20 mg L^{-1} T: 25 °C pH: ~7 Time: 2 h Dose: 15 mg/50 mL λ_{max}: 460 nm	51.74 mg g^{-1}	Pseudo-second-order kinetics; Langmuir isotherm; external diffusion, boundary layer diffusion, and intra-particle diffusion
Magnetite-loaded multi-walled carbon nanotubes[170]	MB	C_0: 20 mg L^{-1} Dose: 0.02 g/50 mL T: 25 ± 1 °C pH: 7	48.06 mg g^{-1}.	Pseudo-second-order kinetics; Langmuir isotherm; electrostatic attraction and π–π stacking interactions
Magnetite/MWCNTs[169]	MB	C_0: 10–70 mg L^{-1} Dose: 0.02 g/25 mL Time: 0–11 min pH: 1	55 mg g^{-1}	Pseudo-second-order kinetics; Langmuir isotherm; electrostatic interactions, π–π dispersion interaction, hydrogen bonding, and electron donor–acceptor complex formation.
Graphene oxide, reduced graphene oxide, and their nanocomposites				
3D hierarchical GO–NiFe LDH composite[178]	CR and MO	Time: 225 min and 135 min, respectively	489 and 438 mg g^{-1}, respectively	Pseudo-second-order kinetics; Langmuir isotherm; electrostatic attraction, ions exchange, and π–π stacking interaction
Graphene/PANI/Fe_3O_4[179]	CR	C_0: 100 mg L^{-1} Time: 2 h Dose: 25 mg/25 mL λ_{max}: 625 nm and 498 nm, respectively	248.76 mg g^{-1}	Pseudo-second-order kinetics; Langmuir isotherm; electrostatic interaction, hydrogen bond, and π–π stacking interaction
Graphene oxide[174]	MB	C_0: < 250 mg L^{-1} λ_{max}: 664 nm	714 mg g^{-1}	Freundlich isotherm; exothermal adsorption reaction, and π–π stacking interaction
Layered graphite oxide[180]	MB and MG	Dose: 10 mg/500 mL λ_{max}: 663 nm and 617 nm, respectively	351 mg g^{-1} and 248 mg g^{-1}, respectively	Pseudo-second-order kinetics; Langmuir isotherm; electrostatic attraction
Graphene oxide/magnesium oxide nanocomposites[181]	MB	C_0: 5–100 mg L^{-1} Time: 5–60 min Dose: 0.1–1 g L^{-1} pH: 11 λ_{max}: 664 nm	833 mg g^{-1}	Pseudo-second-order kinetics; Langmuir isotherm; electrostatic attraction, hydrogen bonding, and π–π interaction
GO/Fe_3O_4 nanohybrids[183]	MB	C_0: 20 mg L^{-1} Dose: 3 mg/5 mL pH: 6 λ_{max}: 664 nm	~100%	Adsorption mechanism followed by π–π interaction
Sandwiched Fe_3O_4/carboxylate graphene oxide nanostructures[182]	MB and RhB	C_0: 10 mg L^{-1} MB and 5 mg L^{-1} RhB pH: 6 λ_{max}: 632 nm and 554 nm, respectively	36 mg g^{-1} and 22.1 mg g^{-1}, respectively	Pseudo-second-order kinetics; electrostatic attraction

Table 4 (*continued*)

Adsorbent	Dyes	Experimental conditions	Adsorption capacity/ removal efficiency	Adsorption kinetics, isotherm, and mechanisms
Magnetic GO/poly(vinyl alcohol) composite gels[207]	MB and methyl violet (MV)	Dose: 20 mg/5 mL C_0: 0.2 mM Time: 0.5 h λ_{max}: 662 nm and 583 nm, respectively	270.94 and 221.23 mg g^{-1}, respectively	Pseudo-second-order kinetics, Langmuir isotherm; strong electrostatic attraction and complexation
Hybrids of natural and synthetic clay				
Cross-linked chitosan/ sepiolite clay composite[194]	MB and Reactive orange 16	C_0: 100 mg L^{-1} Dose: 2 g L^{-1} Time: 30 h pH: >9 for MB and 3 for reactive orange 16 λ_{max}: 665 nm and 496 nm, respectively	40.986 mg g^{-1} and 190.965 mg g^{-1}, respectively	Pseudo-second-order kinetics; Freundlich isotherm; physisorption
MgAl-layered double hydroxide supported MOF[195]	MO	Time: 20 min C_0: 5–50 mg L^{-1} λ_{max}: 463 nm	99% and 600 mg g^{-1}	Pseudo-first-order kinetics; electrostatic attraction
Mg–Al-layered double hydroxide[196]	Reactive Red, Congo red, and Acid Red 1	Time: 60 min pH: 9–10 λ_{max}: 543 nm, 500 nm, and 532 nm, respectively	59.49 mg g^{-1}, 37.16 mg g^{-1}, and 108.0 mg g^{-1}, respectively	Pseudo-second-order kinetics; Langmuir isotherm; electrostatic attraction and ion exchange
Nanohybrid layered double hydroxides[197]	Amaranth, diamine Green B, and brilliant green	T: Room temperature pH: 7–9.5 λ_{max}: 520 nm, 623 nm, and 624 nm, respectively	0.8 mmol g^{-1}, 1.089 mmol g^{-1}, and 1.418 mmol g^{-1}, respectively	Pseudo-second-order kinetics; ion exchange
Hybrids of fly ash				
Biomass fly ash geopolymer monoliths[199]	MB	C_0: 1–50 mg L^{-1} Time: 30 h λ_{max}: 664 nm	15.4 mg g^{-1} Reused up to five cycles	Freundlich isotherm; electrostatic attraction
Porous biomass fly ash-based geopolymer spheres[198]	MB	C_0: 10–125 mg L^{-1} Time: 30 h λ_{max}: 664 nm	79.7 mg g^{-1} Reused up to eight cycles	Freundlich isotherm; multilayer adsorption
Fly ash–TiO_2 composite[201]	Mixture of bemacid red and bemacid blue	C_0: 10 mg L^{-1} each pH: 10.6 λ_{max}: 444 nm and 652 nm, respectively	4.003 and 1.194 mg g^{-1}	Pseudo-second-order kinetics; hydrogen abstraction, redox reactions, also the π-bonds
$Ca(OH)_2/Na_2FeO_4$ modified fly ash[202]	Orange II	C_0: 50 mg L^{-1} Dose: 2000 mg L^{-1}	24.8 mg g^{-1}	Pseudo-second-order kinetics; Langmuir isotherm; electrostatic interaction, hydrogen bonding
Hybrids of bio adsorbents				
Cellulose-*g*-poly(acrylic acid-*co*-acrylamide)[204]	Acid blue 93 (AB93) and MB	C_0: 200 mg L^{-1} Time: 90 min. pH: 7 Dose: 0.4 g L^{-1} λ_{max}: 664 and 607 nm, respectively	1602 and 1814 mg g^{-1}, respectively	Pseudo-second-order kinetics, Freundlich isotherm; electrostatic interaction
Sulphonated bio-adsorbent from waste hawthorn kernel[205]	MB	C_0: 25–400 mg L^{-1} Time: 0–360 min T: 25–60 °C Dose: 0.1 g in 50 mL λ_{max}: 665 nm	151.5 mg g^{-1}	Pseudo-second-order kinetics; Langmuir isotherm; ion exchange process
Cross-linked beads of activated oil palm ash zeolite/ chitosan[203]	MB and acid blue 29	C_0: 50–400 mg L^{-1} T: 50 °C pH: 3–13 λ_{max}: 668 and 602 nm, respectively	199.2 mg g^{-1} and 270.27 mg g^{-1}, respectively	Pseudo-second-order kinetics; Freundlich isotherm; physisorption
Agricultural waste/graphene oxide 3D[206]	MB	C_0: 1000 mg L^{-1} T: 25 °C pH: 12 λ_{max}: 663 nm	414.03 mg g^{-1} The removal was >90% after five cycles	Pseudo-second-order kinetics; Temkin isotherm; multimolecular layers of coverage and heterogeneous adsorption

C_0: initial dye concentration; T: temperature; and λ_{max}: maximum wavelength detected for the analysis of dye.

4.4. Metal oxide-based (magnetic and non-magnetic) hybrid materials

In recent years, metal oxide-based nano-adsorbents have been widely applied in wastewater treatment due to their unique attributes such as large surface area, nano-size, high reactivity, high ability to blend, and robust solution mobility.[1,208] Considering this, the performance of various metal oxide-based hybrid materials as adsorbents in dye removal is reviewed below.

4.4.1 Magnetic metal oxide nanocomposites. Magnetic nanomaterials exhibit additional advantages in the separation of the catalyst/adsorbent by applying an external magnetic field.[209] Gao *et al.* used Fe_3O_4/CeO_2 as a magnetic composite for the removal of Acid Black 210. The maximum adsorption capacity (93.1 mg g^{-1}) achieved was six times higher than of the commercial CeO_2. The corresponding experimental data fitted well with the Langmuir isotherm.[210] Fe_3O_4 magnetic nanoparticles, due to their large surface-to-volume ratio and pore size, showed an adsorption capacity of 150–600 mg g^{-1} of Rhodamine 6G in 30 min.[211] At room temperature, the adsorption of MO, Reactive Brilliant Red K-2BP, and Acid Red 18 in contaminated water on an amine/Fe_3O_4-functionalized biopolymer magnetic resin correlated well with the Langmuir adsorption isotherm.[212] The corresponding adsorption capacity values were found to be 222.2, 101.0, and 99.4 mg g^{-1}, respectively. This high adsorption capacity was attributed to the presence of amine groups and the enhanced surface area of amine/Fe_3O_4-resin. In another study, Mg-ferrite magnetic nanoparticles exhibited relatively low adsorption capacity in the removal of methyl green (1.23 mg g^{-1}) and basic fuchsin (2.55 mg g^{-1}).[213] NaOH-treated wheat straw impregnated with Fe_3O_4 nanoparticles achieved a maximum adsorption capacity of 1374.6 mg g^{-1} in the removal of MB from contaminated water.[214] The adsorption process (endothermic) was likely to be dependent on pH and temperature. The adsorption mechanisms were proposed considering the formation of a surface complex and ion exchange between the MB molecules and adsorbent. Further, a γ-Fe_2O_3 nanoadsorbent exhibited equilibrium adsorption of Acid Red 27 dye within 4 min at a low pH (<5.5), and a decrease in the dye removal efficiency was observed with an increase in temperature.[215] The adsorption of Acid Red 27 dye on γ-Fe_2O_3 followed both the Langmuir and Freundlich isotherms.

Mahapatra *et al.* reported a maximum adsorption capacity of 416.66 mg g^{-1} at pH 7 for the adsorptive decolorization of CR dye on an Fe_2O_3–Al_2O_3 nanohybrid. This higher adsorption capacity was primarily due to the interaction of the amine functional group of the CR dye molecules with the oxy-hydroxide group of the nanohybrid material.[216] An Fe–Mn–Zr metal oxide nanocomposite showed a maximum adsorption capacity of 196.07 and 175.43 mg g^{-1} for the adsorption of MO and eosin yellow dyes, respectively.[217] The saturation magnetization of the adsorbent was found to be enough for its rapid magnetic separation from water. Further, the maximum adsorption capacity of 714.29 mg g^{-1} with a contact time of 3 h was achieved by a core@double-shell-structured HNTs/Fe_3O_4/poly(DA + KH550) adsorbent in the removal of MB dye.[218]

4.4.2 Nonmagnetic metal-oxide nanocomposites. Various nonmagnetic oxide hybrid nanomaterials have been applied as adsorbents in the removal of dyes from the contaminated water. According to Li *et al.*, the adsorption capacity of MO on nano-dimensional Co/Cr-codoped ZnO was 1057.9 mg g^{-1} due to its high specific surface area and positive charge on its surface.[219] Lei *et al.* noted a maximum adsorption capacity of 397 mg g^{-1} on ZnO–Al_2O_3 for the removal of CR dye in 12 h. This adsorbent consisted of microspheres a diameter in the range of 12–16 μm, which were assembled by nanosheets with a thickness of nearly 60 nm.[220] The maximum adsorption capacity of 367 mg g^{-1} for methyl blue dye on Ni–MgO hybrid is attributed to the hydrogen bonding between the N-atoms (which have high electron affinity and smaller atom radius) of methyl blue and OH group on the surface of MgO.[221] According to Lei *et al.*, a maximum adsorption capacity of 357 mg g^{-1} was achieved in 12 h for CR dye on NiO–Al_2O_3. This was ascribed mainly to the synergistic effect, high specific surface area, and positive surface charge (at pH 7) of the adsorbent.[222] ZnV_2O_4 hollow spheres comprised of a flower-like structure and a large number of compacted nanosheets, as depicted in the SEM image (Fig. 11), exhibited an adsorption capacity of 153.14 mg g^{-1} in 40 min for MB.[223] Table 5 presents the performance of metal and metal oxide-based hybrid

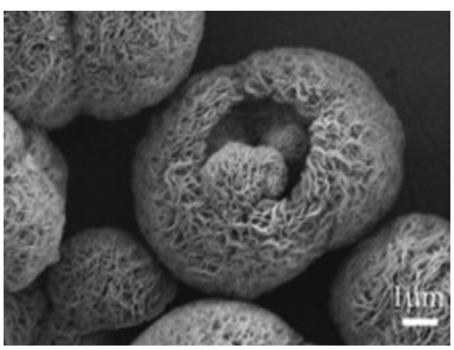

Fig. 11 Morphology of a metal oxide-based adsorbent, ZnV_2O_4 hollow spheres [Reprinted with permission from ref. 223. Copyright 2011, Elsevier].

Table 5 Metal oxide-based hybrid (magnetic and non-magnetic) nanocomposite materials for dye removal

Adsorbent	Dyes	Experimental conditions	Adsorption capacity/ removal efficiency	Adsorption kinetics, isotherm, and mechanisms
Pure magnetic materials				
Fe_3O_4[211]	Rhodamine 6G	pH ~ 7 Dose: 2.5–10 mg L^{-1} Time: 30 min λ_{max}: 525 nm	150–600 mg g^{-1}	Fluorescence resonance energy transfer between the dye molecules and Fe_3O_4 magnetic nanoparticle
γ-Fe_2O_3[215]	Acid red 27	pH < 5.5 Time: 4 min λ_{max}: 520 nm	0.027 mmol g^{-1}	Pseudo-second-order kinetics; Langmuir and Freundlich isotherm; physisorption and electrostatic attraction

Table 5 (*continued*)

Adsorbent	Dyes	Experimental conditions	Adsorption capacity/ removal efficiency	Adsorption kinetics, isotherm, and mechanisms
Magnetic-carbon-based nanocomposite				
Magnetic graphene oxide modified by chloride imidazole ionic liquid[224]	Anionic: Glenn Black R (GR) and Orange IV (OIV) cationic: acridine orange (AO) and crystal violet (CV)	C_0: 40 mg L^{-1} pH: 4 Dose: 0.01 g/25 mL λ_{max}: 520 nm, 440 nm, 490 nm, and 580 nm, respectively	GR, OIV, AO, and CV were 588.24, 57.37, 132.80, and 69.44 mg g^{-1}, respectively	Pseudo-second-order kinetics; Langmuir isotherm; electrostatic interaction
Magnetic graphene oxide freeze-dried[225]	RhB	Dose: 0.007 g/50 mL C_0: 30–80 mg L^{-1} T: 25 °C λ_{max}: 553 nm	126.58 mg g^{-1}	Pseudo-second-order kinetics; Langmuir isotherm; electrostatic interaction
Humic acid–Fe_3O_4[226]	Malachite green (MG)	Dose: 50 mg/50 mL λ_{max}: 618 nm	79.3 mg g^{-1}	Pseudo-second-order kinetics; Freundlich isotherm; electrostatic attraction, π–π interaction, and hydrogen bonding
Magnetic graphene oxide[227]	MB and orange G	Dose: 20 mg/20 mL C_0: 90 and 60 mg L^{-1} Time: 405 min λ_{max}: 667 and 475 nm, respectively	64.23 mg g^{-1} and 20.85 mg g^{-1}, respectively	Pseudo-second-order kinetics; Langmuir isotherm; electrostatic interaction
Fe_3O_4/GO[189]	MB and MO	C_0: 1 mg L^{-1} pH: 6 λ_{max}: 644 and 466 nm, respectively	666.7 and 714.3 mg g^{-1}, respectively	Langmuir isotherm; electrostatic interaction
Magnetic-based metal oxides				
Fe_3O_4/CeO_2[210]	Azo dye (Acid Black 210 (AB210))	Dose: 50 mg/50 mL C_0: 20–400 mg L^{-1} λ_{max}: 461 nm	93.08 mg g^{-1}	Pseudo-second-order kinetics; Langmuir isotherm; chemisorption
Iron oxide–alumina[216]	CR	pH: 7	416.66 mg g^{-1}	Pseudo-second-order kinetics; Freundlich isotherm; multilayer adsorption
Fe–Mn–Zr metal oxide[217]	MO and eosin yellow (EY)	Time: 62 min Dose: 0.45 g L^{-1} C_0 (MO): 11 mg L^{-1}, C_0 (EY): 25 mg L^{-1} λ_{max}: 464 and 517 nm, respectively	196.07 and 175.43 mg g^{-1}, respectively	Pseudo-second-order kinetics; Langmuir isotherm; surface adsorption and pore diffusions
TiO_2/SiO_2/Fe_3O_4 hollow magnetic microspheres[228]	MB	C_0: 20 mg L^{-1} Dose: 0.5 g L^{-1} Time: 50 min	147 mg g^{-1}	Pseudo-second-order kinetics; Langmuir isotherm; electrostatic interaction
Al cation-doped $MgFe_2O_4$[229]	MO	Time: 120 min Dose: 1 g L^{-1}	274.6 mg g^{-1}	Pseudo-second-order kinetics; Langmuir isotherm; electrostatic interaction
CNT/MgO/$CuFe_2O_4$[230]	Methyl violet dye and Nile blue dye	Dose: 1 g L^{-1} C_0: 10 mg L^{-1} λ_{max}: 584 and 638 nm, respectively	36.46 mg g^{-1} and 35.60 mg g^{-1}, respectively	Pseudo-second-order kinetics; Langmuir isotherm; electrostatic interaction
Magnetic Fe_3O_4@UiO-66[231]	MB and MO	Dose: 20 mg/100 mL C_0: 20 mg L^{-1} λ_{max}: 631 and 463 nm, respectively	205 mg g^{-1} and 244 mg g^{-1}, respectively.	Pseudo-second-order kinetics; Langmuir isotherm; electrostatic attraction and π–π stacking interactions
$MgFe_2O_4$[213]	Methyl green (MG) and basic fuchsin (BF)	C_0: 30 mg L^{-1} Dose: 0.8 g L^{-1} λ_{max}: 632 and 541 nm, respectively	1.231 and 2.545 mg g^{-1}, respectively	Pseudo-second-order kinetics; Langmuir isotherm (MG) and Freundlich isotherm (BF); electrostatic interaction (MG) and hydrogen-bond interaction (BF)
$MgFe_2O_4$[232]	MO	C_0: 100 mg L^{-1} Dose: 1 g L^{-1} λ_{max}: 464 nm	181.34 mg g^{-1}	Pseudo-second-order kinetics; Freundlich isotherm; electrostatic forces
Magnetic-based bio-adsorbents				
Fe_3O_4–wheat straw[214]	MB	Dose: 0.01–0.2 g/100 mL pH: 7 λ_{max}: 668 nm	1374.6 mg g^{-1}	Pseudo-second-order kinetics; Freundlich isotherm; complexation formation and ion exchange

Table 5 (*continued*)

Adsorbent	Dyes	Experimental conditions	Adsorption capacity/ removal efficiency	Adsorption kinetics, isotherm, and mechanisms
Fe_3O_4-loaded protonated amine-modified hydrochar[233]	MB and MO	Dose: 40 mg/50 mL C_0: 100 mg L^{-1} T: 303 K λ_{max}: 664 and 464 nm, respectively	148.84 mg g^{-1} (pH 11) and 202.02 mg g^{-1} (pH 5.0), respectively	Pseudo-second-order kinetics; Langmuir isotherm; electrostatic interaction
Magnetic-based polymers				
Core@double-shell structured magnetic halloysite nanotube[218]	MB	C_0: 70–130 mg L^{-1} T: 298 K Time: 3 h	714.29 mg g^{-1} at 318.15 K	Pseudo-second-order kinetics; Langmuir isotherm; complexes formation, electrostatic interaction and π–π stacking interaction
Chitosan–Fe(III) hydrogel[234]	C. I. Acid Red 73 (AR 73)	pH: 12 Time: <10 min C_0: 50 mg L^{-1}	294.5 mg g^{-1}	Pseudo-second-order kinetics; Langmuir–Freundlich isotherm; chemisorption
Fe_3O_4@C@polyaniline trilaminar core–shell[235]	MO	Dose: 8 mg/20 mL C_0: 60 mg L^{-1}	120.2 mg g^{-1}	Pseudo-second-order kinetics; Langmuir isotherm; chemisorption followed by electrostatic attraction and π–π interaction
Fe_3O_4@sodium alginate–Fe(III) polymer gel beads[236]	CR and Direct red 23 (DR 23)	Time: 30 min for CR and 60 min for DR 23 λ_{max}: 498 nm and 502 nm, respectively	3333 and 1429 mg g^{-1}, respectively	Pseudo-second-order kinetics; Langmuir isotherm; electrostatic adsorption, hydrogen bonding, and surface complexation besides van der Waals forces
Magnetic halloysite-based molecularly imprinted polymer[237]	Sunset yellow (SY)	pH: 2 Dose: 0.005 g/0.01 L λ_{max}: 482 nm	46.43 μmol g^{-1}	Pseudo-second-order kinetics; Langmuir isotherm; electrostatic attraction
Sulfonic acid-modified polyacrylamide magnetic composite[238]	Crystal violet (CV) and MB	pH: 10 C_0: 100–4000 mg L^{-1} Dose: 0.5 g L^{-1} Time: 360 min	2106.37 mg g^{-1} and 1462.34 mg g^{-1}, respectively.	Pseudo-second-order kinetics; Langmuir isotherm; electrostatic interaction, hydrogen bonding, and hydrophobic interaction
Fe_3O_4/graphite oxide nanosheet/citric acid-crosslinked β-cyclodextrin polymer[239]	MB	C_0: 50 mg mL^{-1} Dose: 10 mg/25 mL	173 mg g^{-1}	Pseudo-first-order or the intraparticle diffusion model; Sips isotherm; electrostatic attraction, the Lewis acid–Lewis base interaction, the host–guest interaction, and the π–π interaction
Chitosan-fly ash/Fe_3O_4[240]	Reactive Orange 16 (RO16)	pH ~ 4 Dose: 0.08 g T: 303 K Time: 55 min λ_{max}: 493 nm	66.9 mg g^{-1}	Pseudo-second-order kinetics; Freundlich isotherm; electrostatic attraction, dipole–dipole hydrogen bonding interactions, H-bonding, and n–π stacking interactions
Miscellaneous magnetic-based materials				
Magnetic chelated silica particles[241]	Naphthol blue black (NBB) and Eriochrome blue black R (EBBR)	C_0: 0.1 mmol L^{-1} λ_{max}: 618 nm and 569 nm, respectively	3.76 and 1.83 mmol g^{-1}	Pseudo-second-order kinetics; Langmuir isotherm; electrostatic attraction
Ionic liquid grafted-magnetic nanoparticles[242]	Reactive Black 5	C_0: 100 mg L^{-1}	161.29 mg g^{-1}	Pseudo-second-order kinetics; Langmuir isotherm; electrostatic attraction and hydrogen bonding
Magnetic silica nanocomposite-immobilized *Pseudomonas fluorescens*[243]	Rhodamine B	C_0: 50 mg L^{-1} Dose: 1 g L^{-1} pH: 6 λ_{max}: 558 nm	229.6 mg g^{-1}	Pseudo-second-order kinetics; Langmuir isotherm; electrostatic attraction and hydrogen bonding
Water-based ferro fluid[244]	Ponceau S	Ferrofluid dose: 20 mg mL^{-1}	140.26 mg g^{-1}	Pseudo-second-order kinetics; Langmuir isotherm; electrostatic interaction
Clay/starch/Fe_3O_4[245]	Methyl violet (MV)	C_0: 10 mg L^{-1} Dose: 1.5 g L^{-1} pH 9 Time: 150 min T: 298 K	29.67 mg g^{-1}	Pseudo-second-order kinetics; Freundlich isotherm; electrostatic interactions

Table 5 (*continued*)

Adsorbent	Dyes	Experimental conditions	Adsorption capacity/ removal efficiency	Adsorption kinetics, isotherm, and mechanisms
Activated carbon/bentonite/Fe_3O_4[246]	Reactive Red 198	Dose: 2 g L^{-1} C_0: 5 mg L^{-1} pH: 8 Time: 50 min	4.86 mg g^{-1}	Pseudo-second-order kinetics; Langmuir isotherm
Amine/Fe_3O_4-resin[212]	Anionic dye: MO, Reactive Brilliant Red K-2BP, and Acid Red 18	Time: 180 min T: 25 °C pH 2.5, 5.5, and 7.0 respectively	RBR: 101.0 mg g^{-1} MO: 222.2 mg g^{-1} AR: 99.4 mg g^{-1}	Pseudo-second-order kinetics; Langmuir isotherm; chemisorption involved ion exchange
Non-magnetic oxide nanocomposites				
Co/Cr-codoped ZnO[219]	MO	Dose: 10 mg Time: 120 min λ_{max}: 200 nm	1057.90 mg g^{-1}	Pseudo-second-order kinetics; Langmuir isotherm; chemisorption and electrostatic interaction.
ZnO-Al_2O_3[220]	CR	C_0: 50 mg L^{-1} Dose: 10 mg/100 mL Time: 12 h T: 303 K	397 mg g^{-1}	Pseudo-second-order kinetics; Langmuir isotherm; chemisorption
Mesoporous MgO[247]	CR	C_0: 250 mg L^{-1} Dose: 0.02 g/50 mL Time: 60 min	689.7 mg g^{-1}	Pseudo-second-order kinetics; Langmuir isotherm; electrostatic interaction.
MgO/SiO_2[248]	CR	Dose: 10 mg/50 mL C_0: 100 mg L^{-1}–1000 mg L^{-1} T: 25 °C λ_{max}: 498 nm	~4000 mg g^{-1}	Pseudo-second-order kinetics; Langmuir isotherm; electrostatic attractions and surface complexation
MgO–graphene oxide[249]	CR	C_0: 50 mg L^{-1} Dose: 10 mg/50 mL	237 mg g^{-1}	Pseudo-second-order kinetics; Langmuir isotherm; electrostatic and π–π interactions
Ni–MgO[221]	Methyl blue	C_0: 375 mg L^{-1} Dose: 0.1–0.5 g L^{-1} λ_{max}: 600 nm	367 mg g^{-1}	Langmuir isotherm; electrostatic attraction and surface complexation
NiO–Al_2O_3[222]	CR	C_0: 10–100 mg L^{-1} Dose: 10 mg/50 mL Time: 12 h T: 303 K pH: 7	357 mg g^{-1}	Pseudo-second-order kinetics; Langmuir isotherm; positive negative charge attraction
ZnV_2O_4 hollow spheres[223]	MB	C_0: 10 mg L^{-1} Time: 40 min λ_{max}: 664 nm	96% and 153.14 mg g^{-1}	Pseudo-second-order kinetics; Freundlich isotherm; electrostatic attraction

C_0: initial dye concentration; T: temperature; and λ_{max}: maximum wavelength detected for the analysis of dye.

(magnetic and non-magnetic) nanocomposites as adsorbents used in dye removal.

4.5. Metal–organic frameworks

Metal–organic frameworks (MOFs) have attracted much attention as adsorbents due to their fine tuneable pore structures and controllable structures/confined geometries. Besides, the large surface areas, multi-functionality, polar/polarisable bonds, and the possibility of the presence of host–guest interactions through the chemical modification of the organic ligands and/or the inorganic sub-units are also likely to play a unique role.[250–255] According to Li *et al.*, MIL-53(Al)-NH_2 could rapidly bind with MB (208.3 mg g^{-1}) and MG (164.9 mg g^{-1}) due to the hydrogen bonding between the amino groups of the dyes and MOF. Further, MIL-Ti MOFs aided the ultrasound adsorption Basic Red 46, Basic blue 41, and MB from single and binary systems, exhibiting the maximum adsorption capacity of 1250, 1428, and 833 mg g^{-1}, respectively.[257] This high adsorption capacity of MIL-Ti MOFs was attributed to π–π interaction, H-bonding, and electrostatic interaction between the dye molecules and MOFs (Fig. 12). Further, the SEM image of the synthesized NH_2-MIL-125(Ti) having circular plates exhibited the transformation of its morphology due to the effect of the reactant concentration (Fig. 13), which also confirmed the excellent distribution of the nanomaterials. Haque *et al.* developed highly porous MIL-101 MOFs to study the adsorption of MO. The high adsorption capacity of 194 mg g^{-1} depicted the significance of pore size and porosity in the adsorption of MO, following the mechanism of electrostatic interaction on MIL-101.[258]

Further, MIL-100(Fe) and MIL-100(Cr)-derived MOFs were also found to be efficient adsorbents in capturing MO and MB dye molecules from aqueous solution. MIL-100(Fe) showed an adsorption capacity of 1045.2 and 736.2 mg g^{-1}, while that of MIL-100(Cr) was 211.8 and 645.3 mg g^{-1} for MO and MB, respectively.[259] Further, magnetic MOFs have also been used for the adsorption of MB from dye-contaminated water.

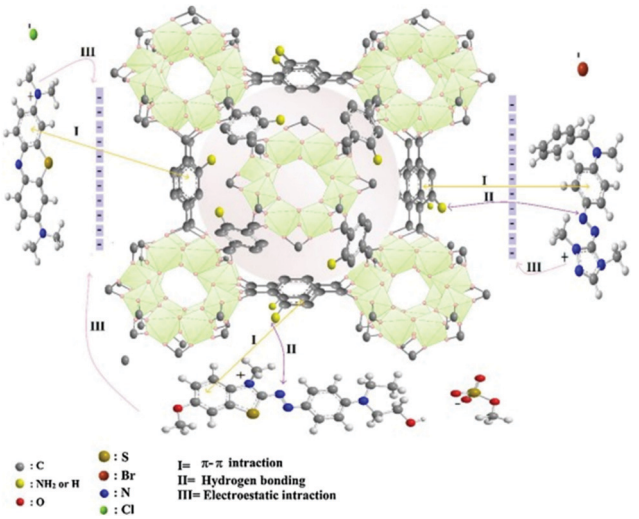

Fig. 12 Multiple dye adsorption mechanisms on MOFs [Reprinted with permission from ref. 257. Copyright 2018, Elsevier].

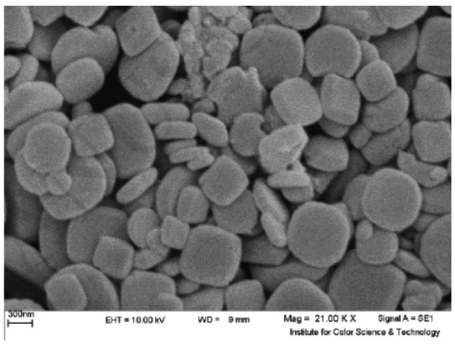

Fig. 13 Morphology of NH_2-MIL-125(Ti) with circular plate [Reprinted with permission from ref. 257. Copyright 2018, Elsevier].

The adsorption mechanism involves hydrophobic interactions and/or π–π interactions between the MB molecules and MOF. It was also noted that the adsorption capacity of a magnetic MOF increased from 84 to 245 mg g^{-1} on increasing the concentration of MB from 30 to 300 mg L^{-1}, respectively.[260] In addition, the adsorption capacity of the zeolitic imidazolate framework comprising ZIF-8, ZIF-8@CNT, and ZIF-8@GO depicted stable and high reusability for over four cycles for the adsorption of MG, corresponding to an adsorption capacity of 1667, 2034, and 3300 mg g^{-1}, respectively.[261] Zhao *et al.* used a zirconium-based metal–organic framework (Zr-MOF) as an adsorbent for the removal of crystal violet and RhB dyes with the maximum adsorption capacity corresponding to 63.38 and 67.73 mg g^{-1}, respectively.[262] Table 6 describes various MOFs used as adsorbents in dye remediation from wastewater.

4.6. Polymers and their nanocomposites

Polymer-based adsorbents, such as polyaniline (PANI), polypyrrole (PPY), PANI/PPY copolymer, PANI/GO, PANI-modified rice husk composites, polymeric rice and Graham flour, polymeric turmeric powder, and chitosan, have found enormous applications in the field of dye treatment due to their easy fabrication, high effective surface area, high selectivity, interesting doping/de-doping chemistry, electrical transport characteristics, strong binding affinities, and porous surface texture.[263–266] For most of the conducting polymer composites, the adsorption of dyes follows the mechanism of physisorption, hydrogen bonding, π–π interactions, and electrostatic interaction.[267] Further, the presence of active groups (*i.e.*, amine and imine) in the polymer facilitates the adsorption process. Many researchers have proposed the applications of polymer-based adsorbents to remediate dyes originating from industrial effluent (Table 7).

Table 6 Metal–organic frameworks (MOFs) for dye removal

MOF	Dyes	Experimental conditions	Adsorption capacity/ removal efficiency	Adsorption kinetics, isotherm, and mechanisms
MIL-53(Al)-NH_2[256]	MB and MG	C_0: 5 mg L^{-1} Dose: 10 mg/100 mL λ_{max}: 663 and 619 nm, respectively	208.3 mg g^{-1} and 164.9 mg g^{-1}, respectively	Langmuir ($R^2 \sim 0.99$) and Freundlich isotherm ($R^2 \sim 0.97$); electrostatic attraction or repulsion.
MIL-Ti[257]	Basic Red 46, basic blue 41, and MB	Time: 30 min pH: 6.3 λ_{max}: 530, 605, and 665 nm, respectively	1250, 1428, and 833 mg g^{-1}, respectively	Pseudo-second-order kinetics; Langmuir isotherm; π–π interaction, hydrogen bonding, electrostatic interactions, and acid–base interactions
Porous MOF material-based on chromium-benzene dicarboxylate[258]	MO	C_0: 30–50 mg L^{-1} λ_{max}: 464 nm	194 mg g^{-1}	Pseudo-second-order kinetics; Langmuir isotherm; electrostatic interaction
MIL-100 (Fe,Cr)[259]	MO and MB	C_0: 400 mg L^{-1}	MIL-100(Cr): MO 211.8 mg g^{-1} MIL-100(Fe): MO 1045.2 mg g^{-1} MIL-100(Cr): MB 645.3 mg g^{-1} MIL-100(Fe): MB 736.2 mg g^{-1}	Pseudo-second-order kinetics; Langmuir isotherm; electrostatic interaction
(Fe_3O_4/Cu_3(BTC))[260]	MB	C_0: 300 mg L^{-1} λ_{max}: 660 nm	245 mg g^{-1}	Pseudo-second-order kinetics; Freundlich isotherm; electrostatic interaction and π–π stacking interaction and/or hydrophobic interactions

Table 6 (*continued*)

MOF	Dyes	Experimental conditions	Adsorption capacity/ removal efficiency	Adsorption kinetics, isotherm, and mechanisms
Zeolitic imidazolate framework (ZIF) ZIF-8, ZIF-8@CNT, ZIF-8@GO[261]	MG	Dose: 0.062, 0.031, and 0.018 g L^{-1} ZIF-8, ZIF-8@CNT, ZIF-8@GO, respectively. Time: 240 min C_0: 50 mg L^{-1} λ_{max}: 618 nm	ZIF-8: 1667 mg g^{-1} ZIF-8@CNT: 2034 mg g^{-1} ZIF-8@GO: 3300 mg g^{-1}	Pseudo-second-order kinetics; Langmuir isotherm; electrostatic interaction
Zirconium-based MOFs[262]	CV and RhB	C_0: 10 mg L^{-1} pH: 11 and 7, respectively. λ_{max}: 585 and 554 nm, respectively.	63.38 mg g^{-1} and 67.73 mg g^{-1}, respectively	Pseudo-second-order kinetics; chemisorption

C_0: initial dye concentration; T: temperature; and λ_{max}: maximum wavelength detected for the analysis of dye.

Table 7 Polymers and their nanocomposites for dye removal

Adsorbent	Dyes	Experimental conditions	Adsorption capacity/removal efficiency	Adsorption kinetics, isotherm, and mechanisms
Pure polyaniline and polypyrrole				
PANI and PPY[61]	CR	C_0: 20 mg L^{-1} pH: 6.55 T: 298 K Dose: 0.4 g L^{-1} and 1.73 g L^{-1}, respectively λ_{max}: 495 nm	250.01 and 66.66 mg g^{-1}, respectively	Pseudo-second-order kinetics; Langmuir isotherm; chemisorption
PPY and PANI[272]	Azo dyes: sunset yellow and CR	pH: 2 λ_{max}: 470 and 497 nm, respectively	212.1 and 147 mg g^{-1}, respectively	π–π electron donor–acceptor interaction and electrostatic attraction
PANI powder[273]	MB	C_0: 3.9 mg L^{-1} λ_{max}: 664 nm	13.854 mg g^{-1}	Pseudo-second-order kinetics; Langmuir isotherm; chemisorption.
PANI[274]	MO	pH: 3 Time: 5 h λ_{max}: 498 nm	92%	
PANI HNTs[275]	MB and acid green	pH: 3–11 λ_{max}: 664 nm and 642 nm, respectively	69.44 and 57.87 mg g^{-1}, respectively	Pseudo-second-order kinetics; Langmuir isotherm; chemisorption involved electrostatic interaction
Polyaniline and polypyrrole based nanocomposites				
PANI/GO and PANI/RGO[280]	MB	Time: 270 min C_0: 50 mg L^{-1} λ_{max}: 660 nm	14.2 and 19.2 mg g^{-1}, respectively	Pseudo-first-order kinetics; Langmuir isotherm; the presence of imine groups and π–π stacking interactions
PANI-modified rice husk composite[281]	Acid red 18	C_0: 40–120 mg L^{-1} λ_{max}: 523 nm	100 mg g^{-1}	Pseudo-second-order kinetics; Langmuir isotherm; chemisorption
PANI/Fe_3O_4[263]	Acid Blue 40	C_0: 50 mg L^{-1} λ_{max}: 620 nm	216.9 mg g^{-1}	Pseudo-second-order kinetics; Freundlich isotherm; electrostatic interaction and H-bond formation
Alpha-cellulose/magnetite/ PPY[282]	Reactive Black 5	pH: 3	62.31 mg g^{-1}	Langmuir isotherm; π–π* interactions, hydrogen bond formation
Starch/polyaniline[278]	Reactive Black and Reactive Violet 4	λ_{max}: 597 and 577 nm, respectively pH: 3	811.30 and 578.39 mg g^{-1}, respectively	Pseudo-second-order kinetics; Toth model; electrostatic interaction
PANI/TiO_2[283]	MB	Dose: 2 g L^{-1} C_0: 400 mg L^{-1} λ_{max}: 664 nm	458.10 mg g^{-1}	Pseudo-second-order kinetics; Temkin isotherm; chemisorption involves membrane diffusion, and intraparticle diffusion
PANI/Starch[279]	MB	C_0: 1–2 × 10^{-5} M Dose: 1.2 g L^{-1}	6.8 × 10^6 mol g^{-1}	Electrostatic interaction
Chitosan-based adsorbents				
Chitosan nanoparticles immobilized on a fibrous carrier[297]	Direct blue-86, photosens, theraphthal, and C.I. Reactive Blue 21	pH: 4–6 C_0: 10–130 mg L^{-1} λ_{max}: 665, 679, 675, and 664 nm, respectively	1097 ± 55, 1049 ± 43, 367 ± 22, and 296 ± 18 mg g^{-1}, respectively	Pseudo-second-order kinetics; Langmuir isotherm; Ion-exchange processes and hydrophobic binding

Table 7 (*continued*)

Adsorbent	Dyes	Experimental conditions	Adsorption capacity/removal efficiency	Adsorption kinetics, isotherm, and mechanisms
Chitosan-based magnetic-adsorbent[64]	Acid orange 7	T: 298 K pH: 6.2 ± 0.2 Dose: 2 g L^{-1} C_0: 50 mg L^{-1} λ_{max}: 485 nm	45.019 mg g^{-1}; 98.01%	Pseudo-second-order kinetics; Sips and Redlich–Peterson isotherm; ion-exchange process
Fe_2O_3–chitosan–bamboo sawdust[298]	Bromothymol blue	Time: 30 min Dose: 0.5 g L^{-1} pH < 7 λ_{max}: 453 nm	217.39 mg g^{-1}	Pseudo-second-order kinetics; Langmuir isotherm; liquid-film and intraparticle diffusion mechanisms
Chitosan–ethylenediamine-tetraacetic acid–magnetic graphene oxide[301]	RhB	Dose: 0.07–0.18 g L^{-1} C_0: 50–250 mg L^{-1} λ_{max}: 554 nm	1085.3 mg g^{-1}	Pseudo-second-order kinetics; Langmuir isotherm; chemisorption and physisorption
Chitosan hydrogel/SiO_2 and chitin hydrogel/SiO_2[299]	Remazol black B, erythrosine B, neutral red, and gentian violet	C_0: 0.05–100 mmol L^{-1}	0.081 mmol g^{-1}, 0.08 mmol g^{-1}, 0.88 mmol g^{-1}, and 0.17 mmol g^{-1}, respectively for chitosan hydrogel/SiO_2, whereas, 0.0062 mmol g^{-1}, 0.15 mmol g^{-1}, 1.06 mmol g^{-1}, and 0.14 mmol g^{-1}, respectively for chitin hydrogel/SiO_2	Freundlich isotherm; physical adsorption
Miscellaneous polymer adsorbents				
Polyvinyl alcohol[300]	Bromothymol blue (BTB) and MB	pH: 6 Time: 10 min λ_{max}: 616 and 664 nm, respectively	276.2 mg g^{-1} and 123.3 mg g^{-1}, respectively 98.65% and 61.32%, respectively	Pseudo-second-order kinetics; Langmuir isotherm; chemisorption
Poly(phenylenediamine) grafted electrospun carbon nanofibers[63]	Coomassie brilliant blue (CBB)	C_0: 100 mg L^{-1} Dose: 5 mg/10 mL Time: 5 h pH: 3 λ_{max}: 555 nm	141 mg g^{-1}	Elovich kinetic; Redlich–Peterson isotherm; electrostatic interaction, π–π interactions, and intermolecular H-bonding

C_0: initial dye concentration; T: temperature; and λ_{max}: maximum wavelength detected for the analysis of dye.

4.6.1 Pure polyaniline and polypyrrole. Polyaniline is one of the most studied conducting polymers due to its many advantages, such as simple synthesis, presence of –NH– groups, capability of doping, excellent physicochemical properties, mechanical flexibility, stability, low cost, and easy availability of its monomer.[101,268] Alternatively, polypyrrole is another polymer studied for the removal of dyes from wastewater.[61] Accordingly, Tanzifi *et al.* studied the adsorption of methyl orange on nano polyaniline at 298 and 338 K. They inferred that an increase in temperature enhanced the adsorption capacity for the dye from 3.34 to 32.04 mg g^{-1} and 3.28 to 30.28 mg g^{-1} corresponding to the initial dye concentration of 10 and 100 mg L^{-1}, respectively. The kinetics and isothermal studies established the pseudo-second-order model and validity of the Langmuir model (maximum monolayer adsorption capacity: 75.9 mg g^{-1}).[269] PANI nanoparticles have also been utilized for the ultrasonication-assisted adsorption of crystal violet dye.[270] The adsorption data fitted well with the Freundlich and Dubinin-Radushkevich isotherms. According to Sharma *et al.*, hyper crosslinked polyaniline (specific surface area: 1083 m^2 g^{-1}) achieved the maximum adsorption capacity of 245 and 220 mg g^{-1} in 60 min for cationic crystal violet and anionic MO dyes in aqueous medium, respectively. These studies also predicted the fitting of the Langmuir adsorption isotherm for both dyes.[271] In another study, the adsorption of CR on PANI and PPY exhibited a maximum adsorption capacity of 250.01 and 66.66 mg g^{-1}, respectively.[61] Further, the experimental results revealed an increase in the adsorption efficiency with reaction time and adsorbent dosage. The kinetic data fitted well with the pseudo-second-order model, while thew equilibrium adsorption findings best correlated with the Langmuir isotherm model. In another study, the adsorption of sunset yellow and CR on a PPY–MWCNT composite achieved an adsorption capacity of 212.1 and 147 mg g^{-1}, respectively.[272] The adsorption mechanism involved electrostatic attraction and π–π electron donor–acceptor interaction. According to Ayad and Zaghlol (2012), cross-linked PANI exhibited an adsorption capacity of 13.85 mg g^{-1} for cationic dyes such as MB (surface area: 349 m^2 g^{-1}). The SEM image of crosslinked polyaniline at high magnification revealed a sponge-like structure, indicating the presence of pores (Fig. 14).[273] Smita *et al.* used PANI to achieve a removal efficiency of 92% in 5 h for a toxic textile dye (MO) present in wastewater. The mechanistic study revealed that the electrostatic interaction between the counterions of the dye molecules and adsorbent was responsible for the adsorption of the dye.[274] The adsorption of MB and acid green dye on PANI hollow nanotubes (internal diameter: 50–60 nm and outer diameter: 5–10 nm) followed the Langmuir model, and their maximum adsorption capacity corresponded to 69.4 and 57.87 mg g^{-1}, respectively.[275] Fig. 15 schematically

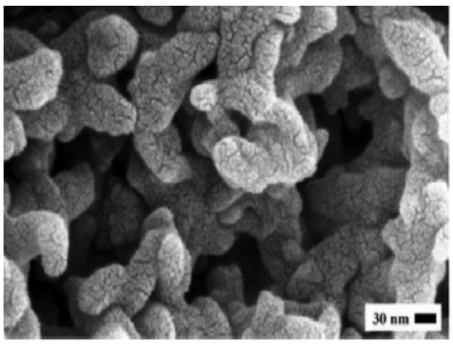

Fig. 14 Scanning electron microscopy image of crosslinked PANI [Reprinted with permission from ref. 273. Copyright 2012, Elsevier].

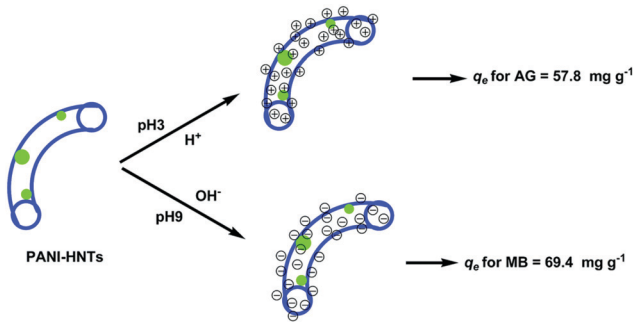

Fig. 15 Schematic illustration of PANI-HNTs at pH 3 and 9 (blue color: PANI-HNTs and green color: AG) [Reprinted with permission from ref. 275. Copyright 2018, The Royal Society of Chemistry].

represents the proposed chemical interaction between PANI hollow nanotubes with MB and acid green dyes at pH of 9 and 3, respectively. MB completely adsorbed on the nanotubes of PANI within 20 min, and the adsorption process well fitted the Langmuir isotherm (maximum adsorption capacity: 9.21 mg g^{-1}).[276] Bhaumik *et al.* reported that the maximum monolayer adsorption capacity of Reactive Black 5 in aqueous solutions (pH 6) was 434.7 mg g^{-1} (318 K) on polyaniline nanofibers (diameter: 50–80 nm). The equilibrium isotherm data fitted the Langmuir isotherm.[277]

4.6.2 Polyaniline and polypyrrole-based nanocomposites. Recently, polymeric nanohybrid materials have attracted significant attention in the field of wastewater treatment due to their high adsorption ability. For example, starch/polyaniline was used to treat reactive black and Reactive Violet 4 dyes, showing an adsorption capacity of 811.30 and 578.39 mg g^{-1}, respectively.[278] The Toth isotherm model better described the single-component equilibrium adsorption, whereas the modified Freundlich model well fitted dye removal. In one study, PANI/starch was used to adsorb MB dye, which shown an adsorption capacity of 6.8 × 10^6 mol g^{-1}.[279] Further, El-Sharkaway *et al.* studied the removal of MB using PANI/GO and PANI/rGO nanocomposites. The adsorption capacity of PANI/GO and PANI/rGO for MB dye was 14.2 and 19.2 mg g^{-1}, respectively, in 270 min.[280] Besides, Shabandokht *et al.* investigated the adsorption of Acid Red 18 dye using a PANI/HCl-modified rice husk composite, which showed an adsorption capacity of 100 mg g^{-1}.[281] This study suggested that the Langmuir adsorption isotherm and pseudo-second-order kinetic model were compatible with the experimental results. In another work, Muhammad *et al.* removed Acid Blue 40 dye using polyaniline, Fe_3O_4, and their composites and the corresponding adsorption capacity was found to be 130.5, 264.9, and 216.9 mg g^{-1}, respectively. The experimental result was better described by the Freundlich isotherm model and the mechanism involved electrostatic interactions and the significant amount of H-bonds present in PANI.[263]

In another study, the adsorption of RB5 dye-cellulose coated with magnetite nanoparticles and conducting PPY followed at pH 3 fitted the Langmuir model well (maximum adsorption capacity: 62.31 mg g^{-1}).[282] Further, Wang *et al.* also used PANI/TiO_2 to remove MB dye with a maximum adsorption capacity of 458.10 mg g^{-1}, and the Langmuir adsorption isotherm well correlated with the experimental results. Chemical adsorption, membrane diffusion, and intraparticle diffusion were the responsible adsorption processes, while H-bonding, electrostatic interaction, and coordination interaction were the responsible adsorption mechanisms (Fig. 16). The attachment of MB on the surface of PANI mainly occurs on amino groups by electrostatic interaction and hydrogen bonding.[283] Thus, a PANI zirconium oxide nanocomposite,[284] PANI nanocomposite functionalized with zirconium(IV) and silicophosphate[285] and PANI α-zirconium phosphate[286] acted as efficient adsorbents for the removal of methylene blue and methyl orange dyes. The adsorption process for the cationic methylene blue dye[287] and Acid Green 25[288] on PANI nanotube/silica was best described by the pseudo-second-order kinetic model and Langmuir adsorption isotherm with the maximum monolayer adsorption capacity of 10.31 and 6.896 mg g^{-1}, respectively. Studies have also been reported

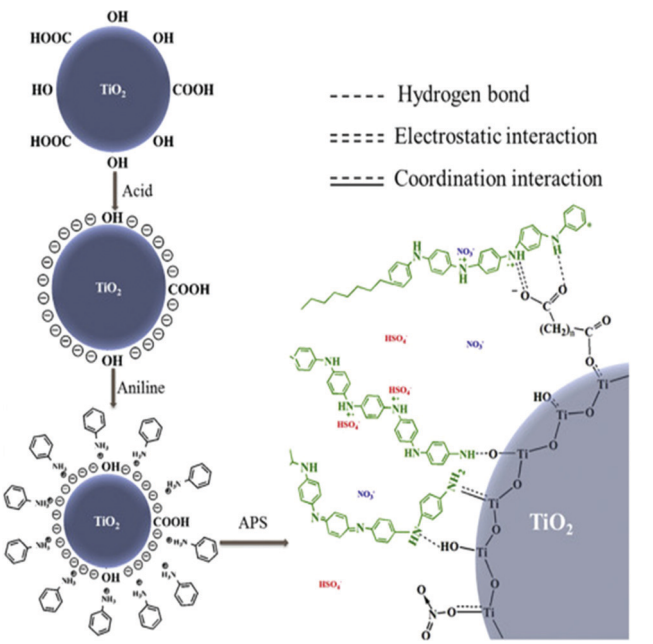

Fig. 16 Schematic showing the adsorption mechanisms of PANI/TiO_2 [Reprinted with permission from ref. 283. Copyright 2019, Elsevier].

using PANI/silver,[289] PANI/alumina,[290] PANI/nickel ferrite,[291] and PANI/zinc ferrite[292] composites for the adsorption of brilliant green dye, anionic dyes (reactive red, Acid Blue 62, and Direct Blue 199), MB, and RhB, respectively.

4.6.3 Chitosan-based adsorbents. Chitosan is considered one of the most economical bio-polymers for dye removal, which can be extracted from natural resources. In comparison to other commercial adsorbents, it has attained great interest due to its unique properties such as cationic charge, high adsorption capacity, macromolecular structure, abundance, and cost-effectiveness.[293,294] Chitosan is also an attractive source of natural polymers for the adsorption of pollutants from wastewater due to its biocompatibility, biodegradability, antibacterial properties, and nontoxicity.[101] However, owing to its poor mechanical properties, low surface area, pH sensitivity, and low porosity, it is generally used in the form of a composite. Considering this, Janaki *et al.* reported that a PANI/chitosan composite efficiently removed Congo red, Coomassie brilliant blue, and Remazol brilliant blue R sulfonated anionic dye with a removal efficiency of 95.4%, 98.2%, and 99.8%, respectively. In contrast, it showed a removal efficiency of only 10.6% for the nonsulfonated cationic dye methylene blue.[295]

The adsorptive removal of Reactive Orange 16 on chitosan/PANI/ZnO agreed well with the Langmuir isotherm and corresponded to a maximum monolayer adsorption capacity of 476.2 mg g^{-1}.[296] In another work, the removal of anionic dyes, namely Direct Blue 86, photosens, theraphthal, and C.I. Reactive Blue 21m was studied on chitosan supported on a fibrous carrier.[297] The experimental data fitted the Langmuir isotherm and showed the maximum adsorption capacity of anionic dye in the range of 300–1050 mg g^{-1} depending on the type, molecular size, and number of anionic groups in the dye. According to Cojocaru *et al.*, spinel ferrite (15%) dispersed in the matrix of chitosan inter-linked with glutaraldehyde, showing an adsorption capacity of 45.02 mg g^{-1} for Acid Orange 7 dye. The hydrogen bonding and hydrophobic interaction between the dye molecules and composite were responsible for the adsorption mechanism.[64] An Fe_2O_3/chitosan-bamboo saw-dust composite efficiently removed the acid dye bromothymol blue.[298] The experimental data well correlated with the Langmuir isotherm model with an adsorption capacity of 217.39 mg g^{-1} achieved in 30 min contact time using 0.5 g L^{-1} adsorbent dose. Copello *et al.* treated Remazol black B, Erythrosine B, neutral red, and gentian violet dyes with chitosan hydrogel/SiO_2 and achieved the maximum adsorption capacity of 0.081, 0.08, 0.88, and 0.17 mmol g^{-1}, respectively.[299]

4.6.4 Miscellaneous polymer-based adsorbents. Agarwal *et al.* used polyvinyl alcohol (PVA) as an adsorbent for the removal of bromothymol and MB from wastewater. The corresponding adsorption isotherms were well fitted with both the Langmuir and Freundlich models. The adsorbent attained the maximum adsorption capacity in 10 min, corresponding to 276.2 and 123.3 mg g^{-1}, respectively.[300] For the adsorption of Coomassie brilliant blue R 250 dye on poly(*para*-, *ortho*- and *meta*-phenylenediamine (PPDA)) grafted electrospun carbon nanofibers, the effective adsorption capacity of 141 mg g^{-1} was achieved and the adsorption kinetics and isotherm data were well correlated with the Elovich kinetic and Redlich–Peterson isotherm models respectively.[63] The adsorption mechanism study suggested electrostatic interaction, π–π interactions, and intermolecular H-bonding controlled the dye sorption. Table 7 shows the removal of dye from contaminated water using conducting polymer, copolymer, and their nanocomposite-based adsorbents. Fig. 17 shows a schematic representation of dye pollution in water and its adsorptive removal using different adsorbents.

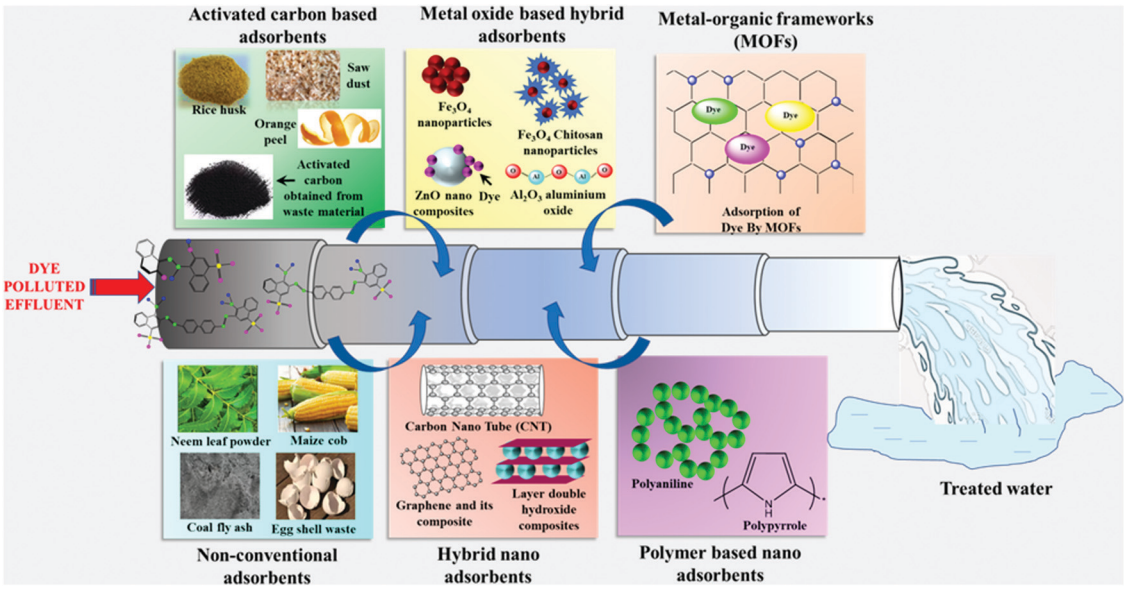

Fig. 17 Schematic presentation of water pollution from dye wastewater, their adsorptive removal using various adsorbents, and the production of treated water.

5. Critical factors influencing dye adsorption

Critical factors such as initial dye concentration, solution pH, temperature, adsorbent dose, and time play a significant role in the adsorptive removal of dyes (Table 8). In this regard, the initial dye concentration makes substantial contributions to the adsorption phenomena. It should be noted that an increase in dye concentration shows positive effects up to a certain limit. Further, the increasing tendency of adsorption for high levels of dye contaminants is directly related to the available active sites on the surface of the adsorbent. The enhanced adsorption capacity is initially accelerated due to the presence of unsaturated active sites in the adsorbent. As the surface of the adsorbent becomes saturated, a considerable reduction in the adsorption of dye occurs.[14,302] According to Mane and Babu (2011), for brilliant green dye with an initial concentration of 100 mg L^{-1}, sodium hydroxide treated saw-dust exhibited an adsorption capacity of 55.86 mg g^{-1}.[121] In another work, the adsorption capacities of 1602 and 1814 mg g^{-1} were recorded on cellulose-*g*-poly(acrylic acid-*co*-acrylamide) as an adsorbent for the initial concentration of acid blue and MB of 200 mg L^{-1}, respectively.[204] These observations suggest, in general, a high initial concentration results in a high adsorption capacity. In addition, the solution pH also plays an essential role in the adsorption of dye from contaminated water. According to Zhou *et al.*, a variation in pH can affect the possible reactions between dye molecules and adsorbents due to the change in the ionization level and surface charge of the adsorbent.[14] In general, low and high solution pH favor the adsorption of anionic and cationic dyes, respectively.[303] This was substantiated by Daneshvar *et al.* and Phoemphoonthanyakit *et al.*, where they reported an adsorption capacity of 1093 mg g^{-1} at pH 2 for Acid Blue 25 and 600 mg g^{-1} at pH 7 for Rhodamine 6G.[142,211] Further, the temperature has a prominent effect on the adsorption of dyes. Additionally, a variation in temperature is also helpful in identifying if adsorption process is endothermic or exothermic. In an exothermic process, the adsorption capacity decreases an increase in temperature, whereas it increases with an increase in temperature in an endothermic process.[304]

In general, an increase in the adsorbent dose has positive effects on the adsorptive removal of dyes, mainly due to the increment in the active sorption sites.[303] In contrast, a higher dose may cause congestion in active sites of the adsorbent. Khan and Nazir (2015) achieved an adsorption capacity of 217.39 mg g^{-1} for bromothymol blue at a dose of 0.5 g L^{-1} using an Fe_2O_3/chitosan–bamboo saw-dust composite.[298] In contrast, Ebrahimian Pirbazari *et al.* reported an adsorption capacity of 1374.6 mg g^{-1} for MB at a dose of 1.0 g L^{-1} NaOH-treated wheat straw impregnated with Fe_3O_4 nanoparticles.[214] These findings clearly demonstrate the positive effects manifested by an increased adsorbent dosage. Finally, an increase in

Table 8 Critical influencing factors affecting the adsorption process

Critical influencing factor	Salient features	Influence on adsorption	Remarks	Ref.
Initial dye concentration	Showing the dissolved amount of dye in aqueous solution and the amount of dye adsorption are directly related to the active sites present on the surface of the adsorbent.	Increased dye concentration causes an increment in adsorption capacity until the unsaturated active sites of the adsorbent become saturated.	In an aqueous environment, the initial concentration of dye may vary from trace level to mg L^{-1} or even more.	14 and 302
pH of the solution	Has a prominent role in dye adsorption.	A variation in pH affects the reaction between dye molecules and adsorbents because of the change in the ionization level and surface charge of the adsorbents.	The pH of the dye effluent may vary depending on the presence of different types of salts (acidic and basic).	14 and 303
	Controls the degree of electrostatic charges provided by ionized dye molecules and causes the varying rate of adsorptions with changing pH.	In the literature, it has been found that low and high pH favor the adsorption of anionic and cationic dyes, respectively.		
Adsorbent dose	Showing the amount of adsorbent used to remove dye particles.	Generally, an increment in dose provides more active sites, which causes an increase in adsorption capacity.	High dose affects the economy of the treatment process.	95 and 303
	Directly related to the number of active sites available on the surface of the adsorbent.	However, a high dose causes congestion in active sites.		
Temperature	Shows the adsorption nature, whether it is endothermic or exothermic.	An increase in adsorption capacity with an increase in temperature shows the endothermic nature, whereas a decrease in adsorption capacity an increase in temperature shows the exothermic nature of reactions.	In general, an increase in temperature increases the adsorption capacity, but a higher temperature is not desirable.	95 and 304
Reaction time	Shows the contact time between adsorbent and adsorbate.	An increase in contact time causes positive effects on the adsorption until equilibrium among active sites of adsorbent and dye molecules is established.	High reaction time affects the economy of the treatment processes due to an increase in energy requirements.	95

contact time may have a negative and/or positive effects on the adsorptive removal of dyes. When equilibrium is established between the active sites of the adsorbent and dye molecules, a further increment in the reaction time has no involvement in the adsorption. Khan and Nazir (2015) have observed an adsorption capacity of 217.39 mg g^{-1} for bromothymol blue in 30 min on an Fe_2O_3/chitosan–bamboo saw-dust composite.[298] In contrast, an adsorption capacity of 1057.90 mg g^{-1} for MO dye was achieved on a nano-dimensional Co/Cr-codoped ZnO adsorbent in 120 min, indicating that an increase in reaction time has positive effects on the adsorption process.[219]

6. Mechanisms of dye adsorption

The adsorption of dye from contaminated water on the surface of an adsorbent is achieved *via* various adsorption mechanisms, as schematically shown in Fig. 18 and displayed in Tables 2–7. It should be noted that the adsorption of water pollutants on adsorbents is mainly guided by electrostatic attraction, π–π interactions, van der Waals forces, hydrogen bonding, acid–base reactions, and hydrophobic interaction.[1] Shen and Gondal reported that electrostatic and intermolecular interactions govern the adsorption of Rhodamine dye on the surface of the adsorbent.[60] According to Zheng *et al.*, the adsorption of anionic dyes, such as CR and MO on GO–NiFe-LDH, is achieved by electrostatic attraction and ion exchange phenomena.[178]

Furthermore, the ion exchange mechanism involves the exchange of ions between a liquid (dye solution) and solid phase (adsorbent). Ebrahimian Pirbazari *et al.* suggested that two principal mechanisms are involved in removing the MB dye on NaOH-treated wheat straw impregnated with Fe_3O_4, namely the formation of a surface complex and ion exchange between the dye molecule and adsorption surfaces.[214] The formation of a surface complex is a mechanism associated with the adsorption process, which is described by the binding of ions to various surface functional groups available onto the surface of the adsorbent and electrostatic interaction between the adsorbent–adsorbate surfaces. Cojocaru *et al.* proposed that the formation of hydrogen bonds between Acid Orange 7 dye and adsorbents accounts for the adsorption process.[64] According to Siddiqui *et al.*, H-bonds between MB and MnO_2/BC arise due to the interaction between the –OH groups present in MnO_2/BC and the acceptor present in MB molecules.[123] Similarly, π–π bonding/π-effects/π-interactions (non-covalent) involve π systems, where similar to electrostatic interactions, positively charged molecules interact with negatively charged surfaces. Further, the adsorption process can follow more than one mechanism simultaneously. For example, the adsorption of Coomassie Brilliant Blue R 250 dye on the surface of adsorbents is governed by electrostatic interactions, π–π interactions, and intermolecular H-bonding.[63] The probable adsorption mechanisms involved in dye removal are shown in Fig. 18, together with the various adsorption processes.

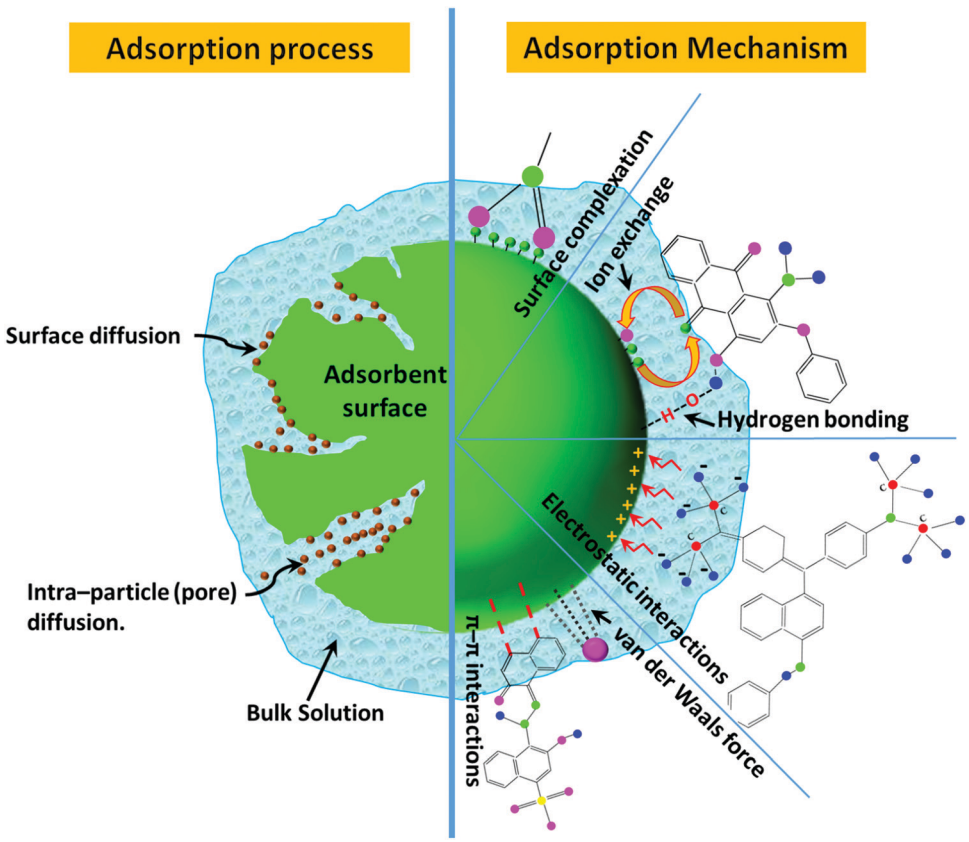

Fig. 18 Adsorption processes and mechanisms for dye removal from bulk liquid.

7. Critiques, future perspectives, and summary

7.1. Critiques and future perspectives

Adsorption is the most preferred technique for dye removal due to its ease of operation, high efficiency, recyclability, and cost-effectiveness. This is also one of the most suitable methods employed for both pilot and field-scale wastewater treatment facilities. The adsorption ability depends on the type of adsorbent used in the removal of dyes from contaminated water. Therefore, adsorbents should have easy availability, cost-effectiveness, high porosity, recycling ability, and abundant active sites on its surface. Recently, commercial adsorbents, such as industrial waste-based adsorbents for the treatment of dyes, pesticides, pharmaceuticals, *etc.*, have received considerable attention due to their involvement in waste minimization. Besides, metal oxide-based adsorbents are also preferred on a large scale due to their unique properties, such as highly active sites and ability to blend with other sorbents. Furthermore, metal–organic framework- and polymer-based adsorbents have also been explored as adsorbents in the treatment of dye-contaminated water owing to their enhanced surface activity and porosity. Considering this, future studies could target the better utilization of commercial and natural bio-adsorbents having good adsorption and desorption capabilities, recyclability, and cost-effectiveness. MOFs and polymer-based adsorbents can be widely researched for wastewater treatment. The adsorption techniques can also be explored in the field of micropollutant remediation such as dyes, pharmaceuticals, and other emerging contaminants at the field scale.

Continuing research is focused on adsorption as one of the prime strategies in the separation of dye from wastewater. However, challenges still exist in developing low-cost, high-performing adsorbents with significantly enhanced activity and long-term stability. In this regard, integrating agro-industrial waste, several naturally existing materials, and eco-friendly industrial waste materials with other biodegradable nanomaterials with no risk to human health and environmental sustainability may be the best alternative. Further, the choice of nanomaterials as adsorbents in wastewater treatment is guided by their high surface area and high adsorption capacity. However, the production cost of nano-adsorbents needs to be considered for their commercial use in any industrial effluent treatment. Despite this, the separation of nanomaterials after adsorption and their disposal are complex and costly processes.[305]

Additionally, cost-effectiveness in terms of reusability of the spent adsorbent should also be considered. Spent adsorbents need to be regenerated and activated by treating them with acid or alkali for their safe and effective reuse.[306] Further, the economical and safe disposal or reuse of spent/exhausted adsorbents need to be considered.[307,308] Dye-loaded spent adsorbents can be utilized to produce biochar materials, fuel cells, for energy production purposes, and also in landfilling.[307,309] Simultaneously, the difficulties and limitations in the scale-up of the treatment technology at the commercial level need to be considered in terms of economic aspects and energy-related issues.

7.2. Summary

The disposal of colored dye wastewater in the environment has depleted freshwater resources and compelled scientists to rethink the availability of clean and safe water. It has been reported that the presence of toxic and colored compounds in dye-containing wastewater results in carcinogenic, mutagenic, allergic, and dermatitis effects on living organisms. This review article reported various classes of dyes and their applications, ecotoxic effects, and sources of dye-contaminated water. The textile, leather, and cosmetic industries were found to be the primary sources of dye-polluted water. Different existing treatment techniques were reviewed and compared for dye removal. Among them, adsorption was selected as a potential technique to treat dye wastewater due to its easy application, simple and scalable synthesis of adsorbents, high removal efficiency, and cost-effectiveness. In this direction, the various adsorbents reported for the removal of dyes from aqueous solution were highlighted. In addition, investigations revealing the adsorption kinetics and fitting of the adsorption isotherm were also presented. MOFs, metal-oxides, and hybrids of bio-adsorbents and carbon show significant adsorption ability for dye contaminants. Various critical factors, such as solution pH, adsorbent dosage, initial dye concentration, temperature, and equilibrium time, were identified as essential factors influencing the adsorption process. Besides, the driving forces responsible for the adsorption of dye molecules are electrostatic interactions, van der Waals forces, hydrogen bonding, and π–π interactions. Thus, the high removal efficiency and field applicability of the adsorption technique make this process suitable for the treatment of dye-contaminated water.

Conflicts of interest

There are no conflicts of interest to declare.

Acknowledgements

S. Dutta and B. Gupta are grateful to the Indian Institute of Technology Kharagpur, India, for financial support.

References

1 F. Lu and D. Astruc, *Coord. Chem. Rev.*, 2020, **408**, 213180.
2 J. K. H. Wong, H. K. Tan, S. Y. Lau, P. S. Yap and M. K. Danquah, *J. Environ. Chem. Eng.*, 2019, **7**, 103261.
3 S. Benkhaya, S. M'rabet and A. El Harfi, *Inorg. Chem. Commun.*, 2020, **115**, 107891.
4 J. Chen, Y. Xiong, M. Duan, X. Li, J. Li, S. Fang, S. Qin and R. Zhang, *Langmuir*, 2020, **36**, 520–533.
5 C. Sahoo, A. K. Gupta and A. Pal, *Desalination*, 2005, **181**, 91–100.
6 C. Sahoo and A. K. Gupta, *J. Environ. Sci. Health, Part A: Toxic/Hazard. Subst. Environ. Eng.*, 2015, **50**, 1333–1341.
7 H. Znad, K. Abbas, S. Hena and M. R. Awual, *J. Environ. Chem. Eng.*, 2018, **6**, 218–227.

8 C. Sahoo, A. K. Gupta and I. M. S. Pillai, *J. Environ. Sci. Health, Part A: Toxic/Hazard. Subst. Environ. Eng.*, 2012, **47**, 2109–2119.
9 E. Guerra, M. Llompart and C. Garcia-Jares, *Cosmetics*, 2018, **5**, 47.
10 N. R. J. Hynes, J. S. Kumar, H. Kamyab, J. A. J. Sujana, O. A. Al-Khashman, Y. Kuslu, A. Ene and B. Suresh Kumar, *J. Cleaner Prod.*, 2020, **272**, 122636.
11 M. Rafatullah, O. Sulaiman, R. Hashim and A. Ahmad, *J. Hazard. Mater.*, 2010, **177**, 70–80.
12 C. Sahoo, A. K. Gupta and I. M. Sasidharan Pillai, *J. Environ. Sci. Health, Part A: Toxic/Hazard. Subst. Environ. Eng.*, 2012, **47**, 1428–1438.
13 S. Senapati, S. K. Srivastava, S. B. Singh and A. R. Kulkarni, *Environ. Res.*, 2014, **135**, 95–104.
14 Y. Zhou, J. Lu, Y. Zhou and Y. Liu, *Environ. Pollut.*, 2019, **252**, 352–365.
15 A. Gičević, L. Hindija and A. Karačić, *IFMBE Proceedings*, Springer Verlag, 2020, vol. 73, pp. 581–587.
16 A. Ghosal, J. Shah, R. K. Kotnala and S. Ahmad, *J. Mater. Chem. A*, 2013, **1**, 12868–12878.
17 C. J. Ogugbue and T. Sawidis, *Biotechnol. Res. Int.*, 2011, **2011**, 1–11.
18 A. Nasar and F. Mashkoor, *Environ. Sci. Pollut. Res.*, 2019, **26**, 5333–5356.
19 K. Deering, E. Spiegel, C. Quaisser, D. Nowak, S. Rakete, M. Garí and S. Bose-O'Reilly, *Environ. Res.*, 2020, **184**, 109271.
20 E. Von Lau, S. Gan, H. K. Ng and P. E. Poh, *Environ. Pollut.*, 2014, **184**, 640–649.
21 B. Lellis, C. Z. Fávaro-Polonio, J. A. Pamphile and J. C. Polonio, *Biotechnol. Res. Innov.*, 2019, **3**, 275–290.
22 M. T. Yagub, T. K. Sen, S. Afroze and H. M. Ang, *Adv. Colloid Interface Sci.*, 2014, **209**, 172–184.
23 N. Nippatla and L. Philip, *Process Saf. Environ. Prot.*, 2019, **125**, 143–156.
24 K. Meerbergen, S. Crauwels, K. A. Willems, R. Dewil, J. Van Impe, L. Appels and B. Lievens, *J. Biosci. Bioeng.*, 2017, **124**, 668–673.
25 B. Dong, H. Chen, Y. Yang, Q. He and X. Dai, *Desalin. Water Treat.*, 2014, **52**, 4562–4567.
26 K. Rachna, A. Agarwal and N. Singh, *Mater. Today: Proc.*, 2019, **12**, 573–580.
27 A. Ahmadi Zahrani and B. Ayati, *J. Electroanal. Chem.*, 2020, **873**, 114456.
28 M. Shaban, M. R. Abukhadra, A. Hamd, R. R. Amin and A. Abdel Khalek, *J. Environ. Manage.*, 2017, **204**, 189–199.
29 S. Samsami, M. Mohamadi, M. H. Sarrafzadeh, E. R. Rene and M. Firoozbahr, *Process Saf. Environ. Prot.*, 2020, **143**, 138–163.
30 H. C. Tee, P. E. Lim, C. E. Seng, M. A. Mohd Nawi and R. Adnan, *J. Environ. Manage.*, 2015, **147**, 349–355.
31 S. Sonal, D. Ugale and B. K. Mishra, *Mine Water Environ.*, 2021, **1**, 3.
32 B. Gupta, T. Priya and B. Kumar Mishra, *Environ. Eng. Res.*, 2020, **26**, 200234.
33 N. Daneshvar, A. Oladegaragoze and N. Djafarzadeh, *J. Hazard. Mater.*, 2006, **129**, 116–122.
34 T. Priya, A. Tarafdar, B. Gupta and B. K. Mishra, *J. Environ. Sci.*, 2018, **70**, 1–10.
35 A. Majumder, B. Gupta and A. K. Gupta, *Environ. Res.*, 2019, **176**, 108542.
36 C. Manera, A. P. Tonello, D. Perondi and M. Godinho, *Environ. Technol.*, 2019, **40**, 2756–2768.
37 B. Gupta, A. K. Gupta, C. S. Tiwary and P. S. Ghosal, *Environ. Res.*, 2020, 110390.
38 B. Gupta, A. K. Gupta, P. S. Ghosal and C. S. Tiwary, *Environ. Res.*, 2020, 109154.
39 S. K. Kuila, D. K. Gorai, B. Gupta, A. K. Gupta, C. S. Tiwary and T. K. Kundu, *Chemosphere*, 2020, 128780.
40 K. G. Pavithra, P. Senthil Kumar, V. Jaikumar and P. Sundar Rajan, *J. Ind. Eng. Chem.*, 2019, **75**, 1–19.
41 C. Sahoo, A. K. Gupta and A. Pal, *Dyes Pigm.*, 2005, **66**, 189–196.
42 A. K. Gupta, A. Pal and C. Sahoo, *Dyes Pigm.*, 2006, **69**, 224–232.
43 C. Sahoo and A. K. Gupta, *J. Hazard. Mater.*, 2012, **215–216**, 302–310.
44 CPHEEO, *Manual on Sewerage and Sewage Treatment Systems – 2013:Central Public Health & Environmental Engineering Organisation (CPHEEO), Govt of India*, 2013.
45 T. H. Kim, Y. Lee, J. Yang, B. Lee, C. Park and S. Kim, *Desalination*, 2004, **168**, 287–293.
46 S. Dutta, K. Manna, S. K. Srivastava, A. K. Gupta and M. K. Yadav, *Sci. Rep.*, 2020, **10**, 1–14.
47 G. Xiong, B. Bin Wang, L. X. You, B. Y. Ren, Y. K. He, F. Ding, I. Dragutan, V. Dragutan and Y. G. Sun, *J. Mater. Chem. A*, 2019, **7**, 393–404.
48 Y. Xiong, Q. Wang, M. Duan, J. Tan, S. Fang and J. Wu, *Langmuir*, 2018, **34**, 7612–7623.
49 Y. Tong, P. J. McNamara and B. K. Mayer, *Environ. Sci.: Water Res. Technol.*, 2019, **5**, 821–838.
50 K. Dutta and S. De, *J. Mater. Chem. A*, 2017, **5**, 22095–22112.
51 M. R. Awual, *Chem. Eng. J.*, 2015, **266**, 368–375.
52 S. A. El-Safty, M. A. Shenashen, M. Ismael, M. Khairy and M. R. Awual, *Analyst*, 2012, **137**, 5278–5290.
53 M. R. Awual, *Mater. Sci. Eng., C*, 2019, **101**, 686–695.
54 M. R. Awual, *Composites, Part B*, 2019, **172**, 387–396.
55 M. R. Awual, *J. Environ. Chem. Eng.*, 2019, **7**, 103124.
56 M. R. Awual, M. M. Hasan, M. M. Rahman and A. M. Asiri, *J. Mol. Liq.*, 2019, **283**, 772–780.
57 M. R. Awual, *J. Environ. Chem. Eng.*, 2019, **7**, 103378.
58 M. R. Awual, T. Yaita, T. Kobayashi, H. Shiwaku and S. Suzuki, *J. Environ. Chem. Eng.*, 2020, **8**, 103684.
59 M. K. Yadav, D. Saidulu, A. K. Gupta, P. S. Ghosal and A. Mukherjee, *J. Environ. Chem. Eng.*, 2021, **9**, 105203.
60 K. Shen and M. A. Gondal, *J. Saudi Chem. Soc.*, 2017, **21**, S120–S127.
61 H. Chafai, M. Laabd, S. Elbariji, M. Bazzaoui and A. Albourine, *J. Dispersion Sci. Technol.*, 2017, **38**, 832–836.
62 N. Mohammadi, H. Khani, V. K. Gupta, E. Amereh and S. Agarwal, *J. Colloid Interface Sci.*, 2011, **362**, 457–462.

63 B. M. Thamer, A. Aldalbahi, M. Moydeen A, H. El-Hamshary, A. M. Al-Enizi and M. H. El-Newehy, *Mater. Chem. Phys.*, 2019, **234**, 133–145.
64 C. Cojocaru, P. Samoila and P. Pascariu, *Int. J. Biol. Macromol.*, 2019, **123**, 587–599.
65 V. K. Gupta, Suhas, I. Ali and V. K. Saini, *Ind. Eng. Chem. Res.*, 2004, **43**, 1740–1747.
66 S. K. Srivastava, S. Senapati, S. B. Singh and P. K. Raul, *RSC Adv.*, 2016, **6**, 113424.
67 A. K. Sahoo, S. K. Srivastava, P. K. Raul, A. K. Gupta and R. Shrivastava, *J. Nanopart. Res.*, 2014, **16**, 1–17.
68 P. Basnet and Y. Zhao, *J. Mater. Chem. A*, 2014, **2**, 911–914.
69 C. B. Godiya, L. A. Martins Ruotolo and W. Cai, *J. Mater. Chem. A*, 2020, **8**, 21585–21612.
70 J. L. Gong, B. Wang, G. M. Zeng, C. P. Yang, C. G. Niu, Q. Y. Niu, W. J. Zhou and Y. Liang, *J. Hazard. Mater.*, 2009, **164**, 1517–1522.
71 D. A. Yaseen and M. Scholz, *Int. J. Environ. Sci. Technol.*, 2019, **16**, 1193–1226.
72 Pubchem, Home – PubChem Compound – NCBI, https://www.ncbi.nlm.nih.gov/pccompound, (accessed 3 February 2021).
73 K. Yamjala, M. S. Nainar and N. R. Ramisetti, *Food Chem.*, 2016, **192**, 813–824.
74 L. C. Davies, G. J. M. Cabrita, R. A. Ferreira, C. C. Carias, J. M. Novais and S. Martins-Dias, *Ecol. Eng.*, 2009, **35**, 961–970.
75 M. Kashefialasl, M. Khosravi, R. Marandi and K. Seyyedi, *Int. J. Environ. Sci. Technol.*, 2006, **2**, 365–371.
76 K. Jain, D. Madamwar and O. Tiwari, *Mapping of Research Outcome on Remediation of Dyes, Dye Intermediates and Textile Industrial Waste*, 2019.
77 S. Shakoor and A. Nasar, *J. Taiwan Inst. Chem. Eng.*, 2016, **66**, 154–163.
78 H. Xiao, T. Zhao, C. H. Li and M. Y. Li, *J. Cleaner Prod.*, 2017, **165**, 1499–1507.
79 A. C. Jalandoni-Buan, A. L. A. Decena-Soliven, E. P. Cao, V. L. Barraquio and W. L. Barraquio, *Philipp. J. Sci.*, 2010, **139**, 71–78.
80 D. T. Sponza and M. Işik, *Process Biochem.*, 2005, **40**, 2735–2744.
81 S. M. Burkinshaw and Y. A. Son, *Dyes Pigments*, 2010, **87**, 132–138.
82 G. Muthuraman and T. T. Teng, *Prog. Nat. Sci.*, 2009, **19**, 1215–1220.
83 G. L. Baughman and E. J. Weber, *Dyes Pigm.*, 1991, **16**, 261–271.
84 C. D. Raman and S. Kanmani, *J. Environ. Manage.*, 2016, **177**, 341–355.
85 A. A. Shalaby and A. A. Mohamed, *RSC Adv.*, 2020, **10**, 11311–11316.
86 K. R. Millington, K. W. Fincher and A. L. King, *Sol. Energy Mater. Sol. Cells*, 2007, **91**, 1618–1630.
87 M. Berradi, R. Hsissou, M. Khudhair, M. Assouag, O. Cherkaoui, A. El Bachiri and A. El Harfi, *Heliyon*, 2019, **5**, e02711.
88 M. F. Abid, M. A. Zablouk and A. M. Abid-Alameer, *J. Environ. Health Sci. Eng.*, 2012, **9**, 1–9.
89 B. Manu and S. Chaudhari, *Bioresour. Technol.*, 2002, **82**, 225–231.
90 A. K. Yadav, C. K. Jain and D. S. Malik, *J. Sustainable Environ. Res.*, 2014, **3**, 95–102.
91 T. Robinson, G. McMullan, R. Marchant and P. Nigam, *Bioresour. Technol.*, 2001, **77**, 247–255.
92 J. Garvasis, A. R. Prasad, K. O. Shamsheera, P. K. Jaseela and A. Joseph, *Mater. Chem. Phys.*, 2020, **251**, 123040.
93 M. F. Abid, M. A. Zablouk and A. M. Abid-Alameer, *Iran. J. Environ. Health Sci. Eng.*, 2012, **9**, 1–9.
94 R. Singh, M. K. Sinha and M. K. Purkait, *Sep. Purif. Technol.*, 2020, **250**, 117247.
95 V. Katheresan, J. Kansedo and S. Y. Lau, *J. Environ. Chem. Eng.*, 2018, **6**, 4676–4697.
96 D. Saidulu, B. Gupta, A. K. Gupta and P. S. Ghosal, *J. Environ. Chem. Eng.*, 2021, 105282.
97 N. Al-Bastaki, *Chem. Eng. Process.*, 2004, **43**, 1561–1567.
98 S. K. Nataraj, K. M. Hosamani and T. M. Aminabhavi, *Desalination*, 2009, **249**, 12–17.
99 G. Moradi, S. Zinadini and L. Rajabi, *Process Saf. Environ. Prot.*, 2020, **144**, 65–78.
100 S. Senapati, S. K. Srivastava and S. B. Singh, *Nanoscale*, 2012, **4**, 6604–6612.
101 A. Nasar and F. Mashkoor, *Environ. Sci. Pollut. Res.*, 2019, **26**, 5333–5356.
102 K. Y. Foo and B. H. Hameed, *Desalin. Water Treat.*, 2010, **19**, 255–274.
103 S. Sonal, P. Prakash, B. K. Mishra and G. C. Nayak, *RSC Adv.*, 2020, **10**, 13783–13798.
104 X. W. Liu, T. J. Sun, J. L. Hu and S. D. Wang, *J. Mater. Chem. A*, 2016, **4**, 3584–3616.
105 P. K. Malik, *J. Hazard. Mater.*, 2004, **113**, 81–88.
106 C. Djilani, R. Zaghdoudi, F. Djazi, B. Bouchekima, A. Lallam, A. Modarressi and M. Rogalski, *J. Taiwan Inst. Chem. Eng.*, 2015, **53**, 112–121.
107 M. S. Rahman, *Water, Air, Soil Pollut.*, 2021, **232**, 1–14.
108 D. A. Giannakoudakis, G. Z. Kyzas, A. Avranas and N. K. Lazaridis, *J. Mol. Liq.*, 2016, **213**, 381–389.
109 E. Akar, A. Altinişik and Y. Seki, *Ecol. Eng.*, 2013, **52**, 19–27.
110 M. A. Ahmad, N. B. Ahmed, K. A. Adegoke and O. S. Bello, *Chem. Data Collect.*, 2019, **22**, 100249.
111 L. Ding, B. Zou, W. Gao, Q. Liu, Z. Wang, Y. Guo, X. Wang and Y. Liu, *Colloids Surf., A*, 2014, **446**, 1–7.
112 S. S. Lam, R. K. Liew, Y. M. Wong, P. N. Y. Yek, N. L. Ma, C. L. Lee and H. A. Chase, *J. Cleaner Prod.*, 2017, **162**, 1376–1387.
113 A. Khan, X. Wang, K. Gul, F. Khuda, Z. Aly and A. M. Elseman, *Egypt. J. Basic Appl. Sci.*, 2018, **5**, 171–182.
114 B. Szczęśniak, J. Phuriragpitikhon, J. Choma and M. Jaroniec, *J. Mater. Chem. A*, 2020, **8**, 18464–18491.
115 A. H. Jawad, R. A. Rashid, M. A. M. Ishak and L. D. Wilson, *Desalin. Water Treat.*, 2016, **57**, 25194–25206.
116 M. Asadullah, M. Asaduzzaman, M. S. Kabir, M. G. Mostofa and T. Miyazawa, *J. Hazard. Mater.*, 2010, **174**, 437–443.

117 A. T. Ojedokun and O. S. Bello, *Appl. Water Sci.*, 2017, **7**, 1965–1977.
118 T. N. V. de Souza, S. M. L. de Carvalho, M. G. A. Vieira, M. G. C. da Silva and D. do S. B. Brasil, *Appl. Surf. Sci.*, 2018, **448**, 662–670.
119 A. Aichour, H. Zaghouane-Boudiaf, C. V. Iborra and M. S. Polo, *J. Mol. Liq.*, 2018, **256**, 533–540.
120 G. Crini, *Bioresour. Technol.*, 2006, **97**, 1061–1085.
121 V. S. Mane and P. V. V. Babu, *Desalination*, 2011, **273**, 321–329.
122 S. I. Abubakar and M. B. Ibrahim, *Bayero J. Pure Appl. Sci.*, 2019, **11**, 273.
123 S. I. Siddiqui, O. Manzoor, M. Mohsin and S. A. Chaudhry, *Environ. Res.*, 2019, **171**, 328–340.
124 K. G. Bhattacharyya and A. Sarma, *Dyes Pigm.*, 2003, **57**, 211–222.
125 S. Chowdhury, S. Chakraborty and P. Saha, *Colloids Surf., B*, 2011, **84**, 520–527.
126 F. Deniz and S. Karaman, *Chem. Eng. J.*, 2011, **170**, 67–74.
127 M. Peydayesh and A. Rahbar-Kelishami, *J. Ind. Eng. Chem.*, 2015, **21**, 1014–1019.
128 A. K. Jain, V. K. Gupta, A. Bhatnagar and Suhas, *J. Hazard. Mater.*, 2003, **101**, 31–42.
129 L. Li, S. Wang and Z. Zhu, *J. Colloid Interface Sci.*, 2006, **300**, 52–59.
130 A. Bhatnagar and A. K. Jain, *J. Colloid Interface Sci.*, 2005, **281**, 49–55.
131 L. Zhou, H. Zhou, Y. Hu, S. Yan and J. Yang, *J. Environ. Manage.*, 2019, **234**, 245–252.
132 M. A. Abdel-Khalek, M. K. Abdel Rahman and A. A. Francis, *J. Environ. Chem. Eng.*, 2017, **5**, 319–327.
133 W. Gao, S. Zhao, H. Wu, W. Deligeer and S. Asuha, *Appl. Clay Sci.*, 2016, **126**, 98–106.
134 S. C. R. Santos and R. A. R. Boaventura, *Appl. Clay Sci.*, 2008, **42**, 137–145.
135 A. Xue, S. Zhou, Y. Zhao, X. Lu and P. Han, *Appl. Clay Sci.*, 2010, **48**, 638–640.
136 R. Yang, D. Li, A. Li and H. Yang, *Appl. Clay Sci.*, 2018, **151**, 20–28.
137 P. P. Selvam, S. Preethi, P. Basakaralingam, N. Thinakaran, A. Sivasamy and S. Sivanesan, *J. Hazard. Mater.*, 2008, **155**, 39–44.
138 Y. Kismir and A. Z. Aroguz, *Chem. Eng. J.*, 2011, **172**, 199–206.
139 K. El Hassani, B. H. Beakou, D. Kalnina, E. Oukani and A. Anouar, *Appl. Clay Sci.*, 2017, **140**, 124–131.
140 L. Chen, C. Li, Y. Wei, G. Zhou, A. Pan, W. Wei and B. Huang, *J. Alloys Compd.*, 2016, **687**, 499–505.
141 G. L. Dotto, V. M. Esquerdo, M. L. G. Vieira and L. A. A. Pinto, *Colloids Surf., B*, 2012, **91**, 234–241.
142 E. Daneshvar, M. S. Sohrabi, M. Kousha, A. Bhatnagar, B. Aliakbarian, A. Converti and A. C. Norrström, *J. Taiwan Inst. Chem. Eng.*, 2014, **45**, 2926–2934.
143 K. Song, H. Xu, L. Xu, K. Xie and Y. Yang, *Bioresour. Technol.*, 2017, **232**, 254–262.
144 J. Wu, T. Zhang, C. Chen, L. Feng, X. Su, L. Zhou, Y. Chen, A. Xia and X. Wang, *Bioresour. Technol.*, 2018, **266**, 134–138.
145 M. M. Hasan, M. A. Shenashen, M. N. Hasan, H. Znad, M. S. Salman and M. R. Awual, *J. Mol. Liq.*, 2021, **323**, 114587.
146 K. T. Kubra, M. S. Salman, H. Znad and M. N. Hasan, *J. Mol. Liq.*, 2021, **329**, 115541.
147 S. D. Khattri and M. K. Singh, *Water, Air, Soil Pollut.*, 2000, **120**, 283–294.
148 M. P. Da Rosa, A. V. Igansi, S. F. Lütke, T. R. Sant'anna Cadaval, A. C. R. Do Santos, A. P. De Oliveira Lopes Inacio, L. A. De Almeida Pinto and P. H. Beck, *J. Environ. Chem. Eng.*, 2019, **7**, 103504.
149 S. Dogar, S. Nayab, M. Q. Farooq, A. Said, R. Kamran, H. Duran and B. Yameen, *ACS Omega*, 2020, **5**, 15850–15864.
150 A. Amari, H. Gannouni, M. I. Khan, M. K. Almesfer, A. M. Elkhaleefa and A. Gannouni, *Appl. Sci.*, 2018, **8**, 2302.
151 L. C. Paredes-Quevedo, C. González-Caicedo, J. A. Torres-Luna and J. G. Carriazo, *Water, Air, Soil Pollut.*, 2021, **232**, 1–19.
152 A. H. Pinto, J. K. Taylor, R. Chandradat, E. Lam, Y. Liu, A. C. W. Leung, M. Keating and R. Sunasee, *J. Environ. Chem. Eng.*, 2020, **8**, 104187.
153 W. Bessashia, Y. Berredjem, Z. Hattab and M. Bououdina, *Environ. Res.*, 2020, **186**, 109484.
154 H. Zhang, P. Wang, Y. Zhang, B. Cheng, R. Zhu and F. Li, *RSC Adv.*, 2020, **10**, 41251–41263.
155 S. K. Srivastava and V. Mittal, *Hybrid Nanomaterials: Advances in Energy, Environment and Polymer Nanocomposites*, John Wiley & Sons, Inc., Hoboken, NJ, USA, 2017.
156 T. S. Kim, H. J. Song, M. A. Dar, H. J. Lee and D. W. Kim, *Appl. Surf. Sci.*, 2018, **439**, 364–370.
157 S. R. Manippady, A. Singh, B. M. Basavaraja, A. K. Samal, S. Srivastava and M. Saxena, *ACS Appl. Nano Mater.*, 2020, **3**, 1571–1582.
158 L. Meng, X. Zhang, Y. Tang, K. Su and J. Kong, *Sci. Rep.*, 2015, **5**, 1–16.
159 L. Jin, X. Zhao, X. Qian and M. Dong, *J. Colloid Interface Sci.*, 2018, **509**, 245–253.
160 Y. Wang, Y. Li, H. Li, H. Zheng and Q. Du, *J. Polym. Environ.*, 2019, **27**, 1342–1351.
161 M. Kamaraj, N. R. Srinivasan, G. Assefa, A. T. Adugna and M. Kebede, *Environ. Technol. Innov.*, 2020, **17**, 100540.
162 M. Goswami and P. Phukan, *J. Environ. Chem. Eng.*, 2017, **5**, 3508–3517.
163 R. Gong, J. Ye, W. Dai, X. Yan, J. Hu, X. Hu, S. Li and H. Huang, *Ind. Eng. Chem. Res.*, 2013, **52**, 14297–14303.
164 B. Pradhan, S. Roy, S. K. Srivastava and A. Saxena, *J. Appl. Polym. Sci.*, 2015, **132**, 41818.
165 B. Bhuyan, S. K. Srivastava and J. Pionteck, *Polym. Technol. Mater.*, 2019, **58**, 537–546.
166 C. H. Wu, *J. Hazard. Mater.*, 2007, **144**, 93–100.
167 Y. Yao, H. Bing, X. Feifei and C. Xiaofeng, *Chem. Eng. J.*, 2011, **170**, 82–89.
168 K. Sui, Y. Li, R. Liu, Y. Zhang, X. Zhao, H. Liang and Y. Xia, *Carbohydr. Polym.*, 2012, **90**, 399–406.
169 M. Ghaedi, H. Khajehsharifi, A. H. Yadkuri, M. Roosta and A. Asghari, *Toxicol. Environ. Chem.*, 2012, **94**, 873–883.
170 L. Ai, C. Zhang, F. Liao, Y. Wang, M. Li, L. Meng and J. Jiang, *J. Hazard. Mater.*, 2011, **198**, 282–290.

171 L. K. De Assis, B. S. Damasceno, M. N. Carvalho, E. H. C. Oliveira and M. G. Ghislandi, *Environ. Technol.*, 2019, **41**, 2360–2371.
172 V. Sabna, S. G. Thampi and S. Chandrakaran, *Water Sci. Technol.*, 2018, **78**, 732–742.
173 C. M. Bezerra de Araujo, G. Filipe Oliveira do Nascimento, G. Rodrigues Bezerra da Costa, K. Santos da Silva, A. M. Salgueiro Baptisttella, M. Gomes Ghislandi and M. Alves da Motta Sobrinho, *Chem. Eng. Commun.*, 2019, **206**, 1375–1387.
174 S. T. Yang, S. Chen, Y. Chang, A. Cao, Y. Liu and H. Wang, *J. Colloid Interface Sci.*, 2011, **359**, 24–29.
175 M. Sivakumar, S. Yadav, W. S. Hung and J. Y. Lai, *J. Cleaner Prod.*, 2020, **263**, 121498.
176 P. Ranjan, J. Balakrishnan and A. D. Thakur, *Materials Today: Proceedings*, Elsevier Ltd, 2019, vol. 11, pp. 833–836.
177 H. Kalita, H. Tyagi and M. Aslam, *Environ. Sci.: Water Res. Technol.*, 2020, **6**, 963–975.
178 Y. Zheng, B. Cheng, W. You, J. Yu and W. Ho, *J. Hazard. Mater.*, 2019, **369**, 214–225.
179 B. Mu, J. Tang, L. Zhang and A. Wang, *Sci. Rep.*, 2017, **7**, 1–12.
180 P. Bradder, S. K. Ling, S. Wang and S. Liu, *J. Chem. Eng. Data*, 2011, **56**, 138–141.
181 M. Heidarizad and S. S. Şengör, *J. Mol. Liq.*, 2016, **224**, 607–617.
182 R. Guo, T. Jiao, R. Li, Y. Chen, W. Guo, L. Zhang, J. Zhou, Q. Zhang and Q. Peng, *ACS Sustainable Chem. Eng.*, 2018, **6**, 1279–1288.
183 T. Jiao, Y. Liu, Y. Wu, Q. Zhang, X. Yan, F. Gao, A. J. P. Bauer, J. Liu, T. Zeng and B. Li, *Sci. Rep.*, 2015, **5**, 1–10.
184 J. Wang, T. Chen, B. Xu and Y. Chen, *Appl. Sci.*, 2020, **10**, 8529.
185 L. Dhar, S. Hossain, M. S. Rahman, S. B. Quraishi, K. Saha, F. Rahman and M. T. Rahman, *J. Phys. Chem. A*, 2021, **125**, 965.
186 H. Mahajan, S. K. Arumugasamy, A. Panda, V. Sada, M. Yoon and K. Yun, *ACS Omega*, 2020, **5**, 24799–24810.
187 S. Haque, S. Gain, K. Gupta and U. C. Ghosh, *Water Qual. Res. J. Can.*, 2019, **54**, 57–69.
188 S. M. Goodman, R. Bura and A. B. Dichiara, *ACS Appl. Nano Mater.*, 2018, **1**, 5682–5690.
189 M. Khajeh and A. Barkhordar, *J. Appl. Spectrosc.*, 2020, **87**, 701–707.
190 S. K. Sahoo, S. Padhiari, S. K. Biswal, B. B. Panda and G. Hota, *Mater. Chem. Phys.*, 2020, **244**, 122710.
191 A. R. B. Bayantong, Y. J. Shih, D. C. Ong, R. R. M. Abarca, C. Di Dong and M. D. G. de Luna, *Chemosphere*, 2021, **274**, 129518.
192 C. Lv, J. Zhang, G. Li, H. Xi, M. Ge and T. Goto, *Colloids Surf., A*, 2020, **585**, 124147.
193 E. Ruiz-Hitzky, P. Aranda, M. Darder and G. Rytwo, *J. Mater. Chem.*, 2010, **20**, 9306–9321.
194 F. Marrakchi, W. A. Khanday, M. Asif and B. H. Hameed, *Int. J. Biol. Macromol.*, 2016, **93**, 1231–1239.
195 A. Chakraborty and H. Acharya, *Colloids Interface Sci. Commun.*, 2018, **24**, 35–39.
196 R. R. Shan, L. G. Yan, Y. M. Yang, K. Yang, S. J. Yu, H. Q. Yu, B. C. Zhu and B. Du, *J. Ind. Eng. Chem.*, 2015, **21**, 561–568.
197 K. Abdellaoui, I. Pavlovic and C. Barriga, *ChemEngineering*, 2019, **3**, 41.
198 R. M. Novais, J. Carvalheiras, D. M. Tobaldi, M. P. Seabra, R. C. Pullar and J. A. Labrincha, *J. Cleaner Prod.*, 2019, **207**, 350–362.
199 R. M. Novais, G. Ascensão, D. M. Tobaldi, M. P. Seabra and J. A. Labrincha, *J. Cleaner Prod.*, 2018, **171**, 783–794.
200 M. Attari, S. S. Bukhari, H. Kazemian and S. Rohani, *J. Environ. Chem. Eng.*, 2017, **5**, 391–399.
201 A. Duta and M. Visa, *J. Photochem. Photobiol., A*, 2015, **306**, 21–30.
202 M. Gao, Q. Ma, Q. Lin, J. Chang and H. Ma, *Appl. Surf. Sci.*, 2017, **396**, 400–411.
203 W. A. Khanday, M. Asif and B. H. Hameed, *Int. J. Biol. Macromol.*, 2017, **95**, 895–902.
204 L. Liu, Z. Y. Gao, X. P. Su, X. Chen, L. Jiang and J. M. Yao, *ACS Sustainable Chem. Eng.*, 2015, **3**, 432–442.
205 Y. Akköz, R. Coşkun and A. Delibaş, *J. Mol. Liq.*, 2019, **287**, 110988.
206 S. Liu, H. Ge, C. Wang, Y. Zou and J. Liu, *Sci. Total Environ*, 2018, **628–629**, 959–968.
207 Z. Cheng, J. Liao, B. He, F. Zhang, F. Zhang, X. Huang and L. Zhou, *ACS Sustainable Chem. Eng.*, 2015, **3**, 1677–1685.
208 M. Khan, M. N. Tahir, S. F. Adil, H. U. Khan, M. R. H. Siddiqui, A. A. Al-Warthan and W. Tremel, *J. Mater. Chem. A*, 2015, **3**, 18753–18808.
209 K. Manna and S. Kumar Srivastava, *ACS Sustainable Chem. Eng.*, 2017, **5**, 10710–10721.
210 S. Gao, W. Zhang, H. Zhou and D. Chen, *J. Rare Earths*, 2018, **36**, 986–993.
211 S. Phoemphoonthanyakit, P. Seeharaj, P. Damrongsak and K. Locharoenrat, *J. Spectrosc.*, 2019, **2019**, 1–5.
212 W. Song, B. Gao, X. Xu, L. Xing, S. Han, P. Duan, W. Song and R. Jia, *Bioresour. Technol.*, 2016, **210**, 123–130.
213 X. Liu, S. An, X. Zhou, L. Zhang, Y. Zhang, W. Shi and J. Yang, *J. Dispersion Sci. Technol.*, 2014, **35**, 1727–1736.
214 A. Ebrahimian Pirbazari, E. Saberikhah and S. S. Habibzadeh Kozani, *Water Resour. Ind.*, 2014, **7–8**, 23–37.
215 N. N. Nassar, *Sep. Sci. Technol.*, 2010, **45**, 1092–1103.
216 A. Mahapatra, B. G. Mishra and G. Hota, *Ceram. Int.*, 2013, **39**, 5443–5451.
217 N. H. Singh, K. Kezo, A. Debnath and B. Saha, *Appl. Organomet. Chem.*, 2018, **32**, e4165.
218 X. Wan, Y. Zhan, Z. Long, G. Zeng and Y. He, *Chem. Eng. J.*, 2017, **330**, 491–504.
219 Z. Li, Y. Sun, J. Xing, Y. Xing and A. Meng, *J. Hazard. Mater.*, 2018, **352**, 204–214.
220 C. Lei, M. Pi, D. Xu, C. Jiang and B. Cheng, *Appl. Surf. Sci.*, 2017, **426**, 360–368.
221 R. M. Mohamed, A. Shawky and I. A. Mkhalid, *J. Phys. Chem. Solids*, 2017, **101**, 50–57.
222 C. Lei, X. Zhu, Y. Le, B. Zhu, J. Yu and W. Ho, *RSC Adv.*, 2016, **6**, 10272–10279.
223 F. Duan, W. Dong, D. Shi and M. Chen, *Appl. Surf. Sci.*, 2011, **258**, 189–195.

224 H. Wang and Y. Wei, *RSC Adv.*, 2017, **7**, 9079–9089.
225 A. Faghihi, M. H. Vakili, G. Hosseinzadeh, M. Farhadian and Z. Jafari, *Desalin. Water Treat.*, 2016, **57**, 22655–22670.
226 G. Y. Abate, A. N. Alene, A. T. Habte and Y. A. Addis, *J. Polym. Environ.*, 2020, **29**, 967–984.
227 J. H. Deng, X. R. Zhang, G. M. Zeng, J. L. Gong, Q. Y. Niu and J. Liang, *Chem. Eng. J.*, 2013, **226**, 189–200.
228 H. Zhang, X. Li, G. He, J. Zhan and D. Liu, *Ind. Eng. Chem. Res.*, 2013, **52**, 16902–16910.
229 H. Nayebzadeh, F. Naderi and B. Rahmanivahid, *J. Inorg. Organomet. Polym. Mater.*, 2020, **31**, 776–789.
230 R. Foroutan, S. J. Peighambardoust, Z. Esvandi, H. Khatooni and B. Ramavandi, *J. Environ. Chem. Eng.*, 2020, 104752.
231 S. Ahmadipouya, M. Heidarian Haris, F. Ahmadijokani, A. Jarahiyan, H. Molavi, F. Matloubi Moghaddam, M. Rezakazemi and M. Arjmand, *J. Mol. Liq.*, 2021, **322**, 114910.
232 B. Rahmanivahid, F. Naderi and H. Nayebzadeh, *J. Water Environ. Nanotechnol.*, 2020, **5**, 1–16.
233 J. L. Liu, W. C. Qian, J. Z. Guo, Y. Shen and B. Li, *Bioresour. Technol.*, 2021, **320**, 124374.
234 C. Shen, Y. Shen, Y. Wen, H. Wang and W. Liu, *Water Res.*, 2011, **45**, 5200–5210.
235 W. Yao, C. Shen and Y. Lu, *Compos. Sci. Technol.*, 2013, **87**, 8–13.
236 T. Lv and B. Li, *J. Polym. Environ.*, 2020, **29**, 1576–1590.
237 S. Foroughirad, V. Haddadi-Asl, A. Khosravi and M. Salami-Kalajahi, *Polym. Adv. Technol.*, 2021, **32**, 803–814.
238 X. Zheng, H. Zheng, R. Zhao, Z. Xiong, Y. Wang, Y. Sun and W. Ding, *J. Mol. Liq.*, 2020, **319**, 114161.
239 L. W. Jiang, F. T. Zeng, Y. Zhang, M. Y. Xu, Z. W. Xie, H. Y. Wang, Y. X. Wu, F. A. He and H. L. Jiang, *Adv. Powder Technol.*, 2021, **32**, 492–503.
240 A. H. Jawad, N. N. A. Malek, A. S. Abdulhameed and R. Razuan, *J. Polym. Environ.*, 2020, **28**, 1068–1082.
241 S. A. Ahmed and E. M. Soliman, *Appl. Surf. Sci.*, 2013, **284**, 23–32.
242 T. Poursaberi and M. Hassanisadi, *Clean: Soil, Air, Water*, 2013, **41**, 1208–1215.
243 G. J. Joshiba, P. S. Kumar, M. Govarthanan, P. T. Ngueagni, A. Abilarasu and F. Carolin C, *Environ. Pollut.*, 2021, **269**, 116173.
244 J. Chen, Q. Cao and X. Han, *J. Cleaner Prod.*, 2021, **287**, 125003.
245 A. Ansari Mojarad, S. Tamjidi and H. Esmaeili, *Int. J. Environ. Anal. Chem.*, 2020, **00**, 1–22.
246 P. Mirzapour, B. Kamyab Moghadas, S. Tamjidi and H. Esmaeili, *Sep. Sci. Technol.*, 2020, **00**, 1–15.
247 L. Ai, H. Yue and J. Jiang, *Nanoscale*, 2012, **4**, 5401–5408.
248 M. Hu, X. Yan, X. Hu, J. Zhang, R. Feng and M. Zhou, *J. Colloid Interface Sci.*, 2018, **510**, 111–117.
249 J. Xu, D. Xu, B. Zhu, B. Cheng and C. Jiang, *Appl. Surf. Sci.*, 2018, **435**, 1136–1142.
250 E. Haque, V. Lo, A. I. Minett, A. T. Harris and T. L. Church, *J. Mater. Chem. A*, 2014, **2**, 193–203.
251 Z. Wang, J. H. Zhang, J. J. Jiang, H. P. Wang, Z. W. Wei, X. Zhu, M. Pan and C. Y. Su, *J. Mater. Chem. A*, 2018, **6**, 17698–17705.
252 L. L. Liu, J. Chen, Y. Zhang, C. X. Yu, W. Du, X. Q. Sun, J. Lou Zhang, F. L. Hu, Y. Mi and L. F. Ma, *J. Mater. Chem. A*, 2021, **9**, 546–555.
253 S. Begum, Z. Hassan, S. Bräse and M. Tsotsalas, *Langmuir*, 2020, **36**, 10657–10673.
254 E. M. Dias and C. Petit, *J. Mater. Chem. A*, 2015, **3**, 22484–22506.
255 W. Xiang, Y. Zhang, Y. Chen, C. J. Liu and X. Tu, *J. Mater. Chem. A*, 2020, **8**, 21526–21546.
256 C. Li, Z. Xiong, J. Zhang and C. Wu, *J. Chem. Eng. Data*, 2015, **60**, 3414–3422.
257 M. Oveisi, M. A. Asli and N. M. Mahmoodi, *J. Hazard. Mater.*, 2018, **347**, 123–140.
258 E. Haque, J. E. Lee, I. T. Jang, Y. K. Hwang, J. S. Chang, J. Jegal and S. H. Jhung, *J. Hazard. Mater.*, 2010, **181**, 535–542.
259 M. Tong, D. Liu, Q. Yang, S. Devautour-Vinot, G. Maurin and C. Zhong, *J. Mater. Chem. A*, 2013, **1**, 8534–8537.
260 X. Zhao, S. Liu, Z. Tang, H. Niu, Y. Cai, W. Meng, F. Wu and J. P. Giesy, *Sci. Rep.*, 2015, **5**, 1–10.
261 J. Abdi, M. Vossoughi, N. M. Mahmoodi and I. Alemzadeh, *Chem. Eng. J.*, 2017, **326**, 1145–1158.
262 J. Zhao, L. Xu, Y. Su, H. Yu, H. Liu, S. Qian, W. Zheng and Y. Zhao, *J. Environ. Sci.*, 2021, **101**, 177–188.
263 A. Muhammad, A. ul H. A. Shah and S. Bilal, *Materials*, 2019, **12**, 2854.
264 S. Dutta, S. K. Srivastava and A. K. Gupta, *Mater. Adv.*, 2021, **2**, 2431–2443.
265 K. T. Kubra, M. S. Salman and M. N. Hasan, *J. Mol. Liq.*, 2021, **328**, 115468.
266 H. Md. Munjur, M. N. Hasan, M. R. Awual, M. M. Islam, M. A. Shenashen and J. Iqbal, *J. Mol. Liq.*, 2020, **319**, 114356.
267 P. Bober, I. M. Minisy, U. Acharya, J. Pfleger, V. Babayan, N. Kazantseva, J. Hodan and J. Stejskal, *Synth. Met.*, 2020, **260**, 116266.
268 S. Acharya, S. Sahoo, S. Sonal, J. H. Lee, B. K. Mishra and G. C. Nayak, *Composites, Part B*, 2020, **193**, 107913.
269 M. Tanzifi, S. H. Hosseini, A. D. Kiadehi, M. Olazar, K. Karimipour, R. Rezaiemehr and I. Ali, *J. Mol. Liq.*, 2017, **244**, 189–200.
270 M. Saad, H. Tahir, J. Khan, U. Hameed and A. Saud, *Ultrason. Sonochem.*, 2017, **34**, 600–608.
271 V. Sharma, P. Rekha and P. Mohanty, *J. Mol. Liq.*, 2016, **222**, 1091–1100.
272 R. S. Aliabadi and N. O. Mahmoodi, *J. Cleaner Prod.*, 2018, **179**, 235–245.
273 M. Ayad and S. Zaghlol, *Chem. Eng. J.*, 2012, **204–205**, 79–86.
274 J. Smita, J. Dipika and K. Shraddha, *Int. J. Sci. Eng. Manage.*, 2016, **1**, 1–6.
275 W. A. Amer, M. M. Omran, A. F. Rehab and M. M. Ayad, *RSC Adv.*, 2018, **8**, 22536–22545.
276 M. M. Ayad and A. A. El-Nasr, *J. Phys. Chem. C*, 2010, **114**, 14377–14383.
277 M. Bhaumik, R. I. McCrindle, A. Maity, S. Agarwal and V. K. Gupta, *J. Colloid Interface Sci.*, 2016, **466**, 442–451.
278 V. Janaki, K. Vijayaraghavan, B. T. Oh, K. J. Lee, K. Muthuchelian, A. K. Ramasamy and S. Kamala-Kannan, *Carbohydr. Polym.*, 2012, **90**, 1437–1444.

279 M. Bin Yeamin, M. M. Islam, A. N. Chowdhury and M. R. Awual, *J. Cleaner Prod.*, 2021, **291**, 125920.
280 E. A. El-Sharkaway, R. M. Kamel, I. M. El-Sherbiny and S. S. Gharib, *Environ. Technol.*, 2020, **41**, 2854–2862.
281 M. Shabandokht, E. Binaeian and H. A. Tayebi, *Desalin. Water Treat.*, 2016, **57**, 27638–27650.
282 P. E. Díaz-Flores, C. J. Guzmán-Álvarez, V. M. Ovando-Medina, H. Martínez-Gutiérrez and O. González-Ortega, *Desalin. Water Treat.*, 2019, **155**, 350–363.
283 N. Wang, J. Chen, J. Wang, J. Feng and W. Yan, *Powder Technol.*, 2019, **347**, 93–102.
284 S. Agarwal, I. Tyagi, V. K. Gupta, F. Golbaz, A. N. Golikand and O. Moradi, *J. Mol. Liq.*, 2016, **218**, 494–498.
285 V. K. Gupta, D. Pathania, N. C. Kothiyal and G. Sharma, *J. Mol. Liq.*, 2014, **190**, 139–145.
286 L. Wang, X. L. Wu, W. H. Xu, X. J. Huang, J. H. Liu and A. W. Xu, *ACS Appl. Mater. Interfaces*, 2012, **4**, 2686–2692.
287 M. M. Ayad, A. Abu El-Nasr and J. Stejskal, *J. Ind. Eng. Chem.*, 2012, **18**, 1964–1969.
288 M. M. Ayad and A. A. El-Nasr, *J. Nanostruct. Chem.*, 2012, **3**, 1–9.
289 M. A. Salem, R. G. Elsharkawy and M. F. Hablas, *Eur. Polym. J.*, 2016, **75**, 577–590.
290 H. Javadian, M. T. Angaji and M. Naushad, *J. Ind. Eng. Chem.*, 2014, **20**, 3890–3900.
291 M. R. Patil and V. S. Shrivastava, *Desalin. Water Treat.*, 2016, **57**, 5879–5887.
292 K. Rachna, A. Agarwal and N. B. Singh, *Environ. Nanotechnol., Monit. Manage.*, 2018, **9**, 154–163.
293 M. Vakili, M. Rafatullah, B. Salamatinia, A. Z. Abdullah, M. H. Ibrahim, K. B. Tan, Z. Gholami and P. Amouzgar, *Carbohydr. Polym.*, 2014, **113**, 115–130.
294 R. A. A. Muzzarelli, J. Boudrant, D. Meyer, N. Manno, M. Demarchis and M. G. Paoletti, *Carbohydr. Polym.*, 2012, **87**, 995–1012.
295 V. Janaki, B. T. Oh, K. Shanthi, K. J. Lee, A. K. Ramasamy and S. Kamala-Kannan, *Synth. Met.*, 2012, **162**, 974–980.
296 P. Kannusamy and S. Thambidurai, *Colloids Surf., B*, 2013, **108**, 229–238.
297 I. M. Lipatova, L. I. Makarova and A. A. Yusova, *Chemosphere*, 2018, **212**, 1155–1162.
298 T. A. Khan and M. Nazir, *Environ. Prog. Sustainable Energy*, 2015, **34**, 1444–1454.
299 G. J. Copello, A. M. Mebert, M. Raineri, M. P. Pesenti and L. E. Diaz, *J. Hazard. Mater.*, 2011, **186**, 932–939.
300 S. Agarwal, H. Sadegh, M. Monajjemi, A. S. Hamdy, G. A. M. Ali, A. O. H. Memar, R. Shahryari-Ghoshekandi, I. Tyagi and V. K. Gupta, *J. Mol. Liq.*, 2016, **218**, 191–197.
301 N. Nekouei Marnani and A. Shahbazi, *Chemosphere*, 2019, **218**, 715–725.
302 Z. Eren and F. N. Acar, *Desalination*, 2006, **194**, 1–10.
303 M. A. M. Salleh, D. K. Mahmoud, W. A. W. A. Karim and A. Idris, *Desalination*, 2011, **280**, 1–13.
304 A. E. Ofomaja and Y. S. Ho, *Dyes Pigm.*, 2007, **74**, 60–66.
305 S. A. Mazari, E. Ali, R. Abro, F. S. A. Khan, I. Ahmed, M. Ahmed, S. Nizamuddin, T. H. Siddiqui, N. Hossain, N. M. Mubarak and A. Shah, *J. Environ. Chem. Eng.*, 2021, **9**, 105028.
306 S. Homaeigohar, *Nanomaterials*, 2020, **10**, 1–42.
307 D. Harikishore Kumar Reddy, K. Vijayaraghavan, J. A. Kim and Y. S. Yun, *Adv. Colloid Interface Sci.*, 2017, **242**, 35–58.
308 S. Lata, P. K. Singh and S. R. Samadder, *Int. J. Environ. Sci. Technol.*, 2015, **12**, 1461–1478.
309 Y. Feng, D. D. Dionysiou, Y. Wu, H. Zhou, L. Xue, S. He and L. Yang, *Bioresour. Technol.*, 2013, **138**, 191–197.